NACA TN 3391

NATIONAL ADVISORY COMMITTEE FOR AERONAUTICS

TECHNICAL NOTE 3391

FREE-FLIGHT MEASUREMENTS OF TURBULENT-BOUNDARY-LAYER SKIN FRICTION IN THE PRESENCE OF SEVERE AERODYNAMIC HEATING AT MACH NUMBERS FROM 2.8 TO 7.0

By Simon C. Sommer and Barbara J. Short

Ames Aeronautical Laboratory
Moffett Field, Calif.

Washington
March 1955

NATIONAL ADVISORY COMMITTEE FOR AERONAUTICS

TECHNICAL NOTE 3391

FREE-FLIGHT MEASUREMENTS OF TURBULENT-BOUNDARY-LAYER SKIN FRICTION IN THE PRESENCE OF SEVERE AERODYNAMIC HEATING AT MACH NUMBERS FROM 2.8 TO 7.0

By Simon C. Sommer and Barbara J. Short

SUMMARY

Experimental measurements of average skin friction of the turbulent boundary layer have been made on free-flying, hollow-cylinder models at Mach numbers of 2.8, 3.8, 5.6, and 7.0, at conditions of high rates of heat transfer. It has been found that for these high heat-transfer conditions, the ratio of skin friction to incompressible skin friction is approximately 35 percent higher than zero-heat-transfer wind-tunnel data at Mach numbers of 2.8 and 3.8. Although no measurements of skin friction have been made at zero-heat-transfer conditions at very high Mach numbers, the data of the present investigation indicate that this same trend of increasing skin-friction ratio with increasing heat-transfer rates will persist at Mach numbers as high as 7.

The Rubesin and Johnson T' method of calculating skin friction for laminar boundary layers has been modified and compared to the data of this investigation and existing wind-tunnel data for conditions close to zero heat transfer. It has been found that values of skin-friction ratio computed by this method agree well with the experimental values over a wide range of Mach numbers and heat-transfer conditions.

INTRODUCTION

The present state of knowledge of the skin friction of turbulent boundary layers at supersonic speeds is primarily guided by the experimental data that exist. These data are fairly complete for conditions close to zero heat transfer at Mach numbers up to 4.5 (refs. 1 and 2). Unfortunately, there has been little experimental investigation of the effects of heat transfer and further increases in Mach number on skin friction. Theoretical estimates generally agree that skin friction increases with increasing heat transfer from the boundary layer to the wall, and decreases with increasing Mach number (e.g., refs. 3 through 7), but are not generally in agreement quantitatively. Since heat-transfer rates will probably be large under conditions of free flight and since flight speeds of interest extend well beyond a Mach number of 4.5, a

program was initiated in the Ames supersonic free-flight wind tunnel to measure skin friction of the turbulent boundary layer under conditions of large heat transfer and to extend the Mach number range for which skin-friction data are available. The results of this investigation are reported herein.[1]

SYMBOLS

A	ratio of that part of the trip drag which results in removing momentum from the boundary layer to the total drag, $\frac{C_{d_t}}{C_D}$, (see Appendix B), dimensionless
C_D	total-drag coefficient, dimensionless
C_{D_t}	trip-drag coefficient, dimensionless
C_{d_t}	coefficient of that part of the trip drag which results in removing momentum from the boundary layer (see Appendix B), dimensionless
C_F	average skin-friction coefficient, turbulent flow, dimensionless
C_{F_i}	incompressible skin-friction coefficient, turbulent flow, dimensionless
C_{F_L}	average skin-friction coefficient, laminar flow, dimensionless
c_m	specific heat of model material, Btu/lb $^\circ$F
c_p	specific heat of air at constant pressure, Btu/lb $^\circ$F
H	average heat-transfer coefficient, Btu/sec sq ft $^\circ$F
h	wall thickness at base of model, ft
k_m	thermal conductivity of the model material, Btu/sec sq ft $^\circ$F/ft
L	length of run of turbulent flow, ft
l	length of model, ft
M	Mach number, dimensionless
p	static pressure, lb/sq ft

[1]Preliminary results of the present investigation have been presented in reference 8.

p_b base pressure, lb/sq ft

q dynamic pressure, lb/sq ft

R Reynolds number based on model length, dimensionless

R_b, R_c Reynolds numbers used in determining incompressible skin-friction coefficient, dimensionless

R_D Reynolds number based on pipe diameter, subsonic pipe flow, dimensionless

r radius of model from axis to wall center, ft

S surface area, sq ft

S_1 Sutherland constant, $^{\circ}R$

St Stanton number, $\frac{H}{c_{p_1}\rho_1 u_1}$, dimensionless

T absolute temperature, $^{\circ}R$

T_i initial temperature of the model, $^{\circ}R$

t time, sec

u velocity in the x direction of air in the boundary layer, ft/sec

x axial distance, ft

y radial distance, ft

y_1 half-wall thickness, ft

α thermal diffusivity of the model material, $\frac{k_m}{c_m \rho_m}$, sq ft/sec

β_n positive roots of $\beta \tan \beta = \frac{y_1 H}{k_m}$ (values tabulated in Appendix IV, ref. 24), dimensionless

δ boundary-layer thickness, ft

θ boundary-layer momentum thickness, $\int_0^{\delta} \frac{\rho}{\rho_1} \frac{u}{u_1} \left(1 - \frac{u}{u_1}\right) dy$, ft

μ coefficient of viscosity, lb sec/sq ft

ρ density of air, lb/cu ft

ρ_m density of the model material, lb/cu ft

Subscripts

Except where otherwise defined, the following subscripts apply:

o free-stream conditions

1 conditions at the outer edge of boundary layer

w conditions at wall

Superscript

' conditions at which incompressible flow relations must be evaluated in order to represent compressible flow

EQUIPMENT AND TEST CONDITIONS

Skin friction was obtained from measurements of the total drag of spin-stabilized thin-walled tubes of the type shown in figure 1. Test and tare models, identical except for length, were gun-launched under the same conditions, and total-drag coefficients were computed from deceleration data. Deceleration of a model was computed from its time-distance history which was recorded by a chronograph and shadowgraphs (ref. 9). The difference between the total drag of a test model and the total drag of a tare model is, except for small corrections, a measure of the average skin-friction drag of the added length of the test model. This tare-drag method of obtaining skin friction and this hollow-cylinder model configuration were chosen because only small corrections were required for the evaluation of skin friction. In addition, direct correlation could be made with flat-plate results inasmuch as the flow closely resembled two-dimensional flow (boundary-layer thicknesses were small compared to the radius of the cylinder).

Models and Model Launching

The models were made of 75 S-T aluminum, with 1.44 inches outer diameter and 0.030-inch-thick walls. The outer and inner surfaces were polished with successively finer polishing papers, the last being 4/0 polishing paper. The finish of some typical models observed with an interferometer (ref. 10) showed the magnitude of the peak to valley

roughness to be approximately 20 microinches; however, the root-mean-square height of the surface irregularities would be considerably smaller. Three nose contours, a double wedge with a half-angle of 10°, a double wedge with a half-angle of 15°, and a circular-arc profile with a tangent half-angle at the tip of 20°, each having a leading-edge thickness less than 0.001 inch were used. Boundary-layer trips (fig. 2), used throughout to promote turbulent flow over the surface of the models, will be discussed later.

The test models were 2.0 and 2.5 inches long. Tare models were 0.5 inch long. Longer test models were desired to produce a higher percentage of skin friction to total drag, but the model lengths were limited by two factors. At the lower Mach numbers, the model length was limited to 2.0 inches to prevent the shock wave from the leading edge from impinging on the inside of the cylinder wall and causing interference with the boundary-layer flow. This limitation was of no consequence at the higher Mach number because of the smaller shock-wave inclination angle, but models over 2.5 inches long failed structurally due to extremely high acceleration loads encountered in the gun.

The models were launched from a standard 37-mm rifled gun, the twist of the rifling being one turn in three feet corresponding to a helix angle of approximately 7.5°. The models, which were approximately 0.02 inch smaller than the land diameter of the gun, were protected from the rifling by plastic film wrappers which broke away from the models as they emerged from the gun. A rifled aluminum disc, used to produce spin, was followed by a Neoprene seal which prevented powder gas leakage. A test-model assembly is illustrated in figure 3. Muzzle velocities of 3200 and 4400 feet per second were obtained by varying the powder charges and resulted in peak accelerations of 130,000 and 250,000 g's on the models. The structural failure mentioned previously was observed on models 2.5 inches long at accelerations above 300,000 g's.

Test Conditions

Tests were conducted at nominal Mach numbers of 2.8 and 3.9 by firing through still air at one atmosphere pressure where the free-stream static temperature was equal to ambient temperature. A nominal Mach number of 7.2 was obtained by firing upstream through a Mach number 2 air stream where the free-stream[2] static temperature was about 56 percent of the ambient temperature. The free-stream Reynolds number range for the tests was from 3×10^{6} to 9×10^{6}. The actual free-stream Mach numbers and Reynolds numbers of these tests are listed in columns (1) and (2) of table I. It is shown in columns (3) and (4) that the Mach numbers and Reynolds numbers at the outer edge of the boundary layer, denoted by the

[2]Free-stream conditions, as used herein, are the properties of air corresponding to a stationary model in an airstream at the nominal Mach number of the test.

subscript 1, are lower than the free-stream values. These changes were due to the flow over the nose profiles and were calculated by two-dimensional shock-expansion theory which entails simply the calculation of flow at the nose tip with the oblique-shock-wave equations and flow downstream of the nose tip with the Prandtl-Meyer expansion equations. It has been shown in reference 11 that this method is applicable over almost the entire region of completely supersonic flow. The calculated static pressure at the beginning of the cylinder was very nearly equal to free-stream static pressure. It was assumed that the static pressure had returned to free-stream value at the surface trailing edge. In order to represent conditions over the entire cylinder, the mean static pressure was used to calculate the values of M_1 and R_1 listed in table I.

The high-heat-transfer conditions of the tests are implied by the difference between recovery temperatures which were of the order of 1300° to 3200° R and the initial wall temperature of approximately 530° R inasmuch as the wall-temperature rise during the short flight time of 0.01 second was only about 15° to 45°. The heat-transfer conditions are indicated by the difference between columns (9), T_r/T_1, and (8), T_w/T_1, of table I. The values listed in column (8) were estimated theoretically by the method explained in Appendix A. The values listed in column (9) were calculated using a recovery factor of 0.89.

Boundary-Layer Trips

Boundary-layer trips were applied to the inside and outside surfaces of each model to insure a turbulent boundary layer over the model surfaces. The types of trips used are illustrated in figure 2 and consisted of threads and raised wedges continuous around the circumference of the models. These two-dimensional boundary-layer trips, although not as effective as three-dimensional trips, could be more easily reproduced and machined more accurately than any type of three-dimensional roughness. The trip strength for each test condition was varied until the least disturbance which consistently caused turbulence to occur on or near the trailing edge of the roughened region was found; that is, until no laminar flow was observed in the shadowgraphs behind the trailing edge of the trip. For illustration, figure 4 shows a comparison between the type of flow observed when a trip of 0.003-inch-deep threads was used (fig. 4(a)) and when a trip of 0.001-inch-deep threads was used (fig. 4(b)) at a Mach number of 3.9. Careful examination of figure 4(a) reveals Mach waves produced by the turbulent boundary layer as far forward as the shock wave from the trip, indicated by the leader. The Mach waves do not appear in figure 4(b), and moreover, with closer observation it can be seen that the boundary layer over the surface of the model is laminar and turbulence probably started in the annular wake; therefore, the boundary layer between the leading edge and the 0.003-inch-deep trip was necessarily laminar and transition from laminar to turbulent flow occurred somewhere on the trip. It is interesting to note the shock patterns associated with the inside and outside flows and that there is no shock impingement on the boundary layer.

A model with 0.003-inch threads, the type which produced turbulent flow at $M_o = 3.9$ (fig. 4(a)), was tested at $M_o = 7.2$ and $R_o = 7 \times 10^6$, and it was found that the boundary layer was completely laminar. This was particularly surprising since the former test was conducted in still and therefore disturbance-free air, whereas the latter test was run in the presence of air-stream turbulence and shock waves. When the strength of the trip was increased from 0.003-inch to 0.010-inch-deep threads, there was partial laminar flow over the surface of the model. Even a single annular ring of the type shown in figure 2(c), raised 0.010 inch above the surface was not satisfactory, but it was found that the double annular ring 0.008 inch high (fig. 2(c)) consistently produced turbulence in the vicinity of the trip. It was also found that 0.006-inch-deep threads on a circular-arc nose profile (fig. 2(b)) would consistently produce turbulence in the vicinity of the trip. The effect on Mach number of using the circular-arc nose profile was to reduce M_1 to 5.6.

DATA REDUCTION

For a more general comparison of these data with results of theory and experiment, it was necessary that the ratio of skin friction to incompressible skin friction, C_F/C_{F_i}, be presented. It was therefore required that both the skin friction and the corresponding incompressible skin friction be determined.

Determination of Skin-Friction Coefficient

Skin-friction drag was obtained by subtracting the total drag of a tare model from the total drag of a test model. The measured total drags had to be adjusted because of small variations in model geometry and test conditions between test and tare models. These adjustments to total drags were made by determining the differences in individual drag components of a test-tare combination. These differences were obtained from available theoretical and experimental information and are detailed in the following paragraphs. The total effect of making the aforementioned adjustments to the total-drag data changed the skin-friction results, that is, the test minus tare drag, by only 5 percent and noticeably decreased the spread of the total-drag data.

Base drag.- Because of the difference in the lengths of the test and tare models, the boundary-layer thickness at the trailing edge was different, and accordingly the base drag was different; consequently, the base drag had to be adjusted to account for this difference in boundary-layer thickness. The data of Chapman, Wimbrow, and Kester (ref. 12) for blunt trailing-edge wings are reproduced in figure 5(a). These data, extrapolated to a Mach number of 8, are cross plotted in figure 5(b). Although the extrapolation appears somewhat arbitrary, it

is to be emphasized that at the very high Mach numbers, the base drag is only a very small percentage of the total drag, so that fairly large errors could be accepted without introducing significant errors in skin friction. If the extrapolation is in error by as much as 20 percent at the high Mach numbers, this would result in a change of the final skin friction of the order of 1 percent. The values of base drag are better known at the lower Mach numbers as little or no extrapolation is necessary in figure 5. An error in the base-drag corrections of 10 percent at these Mach numbers would result in a change of the final skin friction of the order of only 1.5 percent.

Wave drag.- Wave drag consisted primarily of two components, drag due to leading-edge thickness and drag due to nose profile.

Leading-edge thickness had to be measured very carefully since the drag associated with leading-edge thickness ranged from 8 percent to 16 percent of the skin-friction drag. A metallurgical microscope at X500 was used to measure the leading edges since the thicknesses ranged from 0.0003 to 0.0010 inch from model to model. The leading edges were ground flat to insure uniformity and to improve the accuracy with which they could be measured. The drag associated with leading-edge thickness was calculated with the aid of tables in reference 13 and the assumption that the pressure on the frontal area was the arithmetic mean of the total pressure and static pressure behind a normal shock wave.[3] The maximum error in the measurements of leading-edge thickness could cause 25-percent change in the corrections due to differences in leading-edge drag which would result in 1.5-percent change in the final skin friction.

Small differences occurred in wedge angle and circular-arc profile. The wave drag due to the nose profile of each model was calculated by the shock-expansion method, and corrections were applied for the geometric differences that were measured. The maximum error in the measurements of geometry could cause 10-percent change in these corrections which would result in negligible change (0.4 percent) in the final skin friction.

---

[3]This method of calculating the leading-edge drag was confirmed experimentally. A 0.5-inch-long hollow-cylinder model having a double wedge with a 10° half-angle, 0.125-inch-thick wall, and leading-edge thickness of 0.064 inch was tested at a Mach number of 3 and Reynolds number of 10^6. The sum of the estimated base drag, laminar skin friction, and pressure drag on the 10° wedge were only 20 percent of the measured total drag. The remaining 80 percent of the total drag was the drag due to the leading-edge bluntness. This component of drag corresponded to an average pressure on the frontal area which was the mean of the total pressure and static pressure behind a normal shock wave. If either the total pressure or the static pressure behind a normal shock wave were used to evaluate leading-edge drag, the estimated total drag would have differed from the measured value by ±10 percent; whereas, if the mean pressure were used, the estimated total drag would have been only 1 percent different than the measured value.

Drag due to angle of attack.- The attitude history of each model in flight was determined from the shadowgraphs, and the angle of attack was plotted along the flight path. The mean-square angle of attack determined from these plots was multiplied by the lift-curve slope to give the increment of drag necessary to adjust the total drag to that of a model at zero angle of attack. The maximum increment of drag due to lift was so small that a 20-percent change in the correction applied would result in negligible change (0.5 percent) in the final skin friction. It is interesting to note that no visible differences in boundary-layer thickness around the model were ever observed in the shadowgraphs at any angle of attack which occurred in the test program.

Drag due to boundary-layer trips.- Differences in the height of the boundary-layer trips were of the order of 0.0003 inch. Corrections due to these differences could not be ascertained quantitatively. Although it was assumed that the drag due to the trip on a tare model was equal to the drag of the trip on a test model and no corrections were applied, the differences in drag due to the geometric differences of the trips may have been significant. The effect on skin friction of disregarding the possible differences in trip drag will be discussed in the section on test results.

Determination of Incompressible Skin-Friction Coefficient

The effective point of origin of the turbulent boundary layer must be known in order to determine the Reynolds numbers associated with experimental skin friction and to calculate the corresponding incompressible skin-friction coefficient. The position of the effective turbulent origin can be calculated by assuming the momentum thickness of the turbulent boundary layer equal to that of the laminar boundary layer at the transition point. When the boundary-layer trips are small, this method is believed to be valid and was applied as described in Appendix B. It was found, however, that very large trips were necessary at the higher Mach numbers to insure the occurrence of turbulence in the vicinity of the trip. In this case the assumption of equal laminar and turbulent momentum thicknesses at the transition point is unjustified. The effects of such large trips were investigated, and the methods used to treat these cases are reported in the Results and Discussion section.

The incompressible skin-friction coefficient was determined from the Kármán-Schoenherr equation by the following method. The effective turbulent origin was calculated with the assumption that the momentum thicknesses of the laminar and turbulent boundary layers were equal at the transition point which was estimated to be at the midlength of the trip (see Appendix B). Knowledge of the position of the effective turbulent origin was applied to determine the Reynolds numbers required in computing the incompressible skin-friction coefficient. The experimentally

determined skin-friction coefficient was based on the area included between the indicated points b and c of the sketch; thus, the incompressible skin-friction coefficient based on the same area was required.

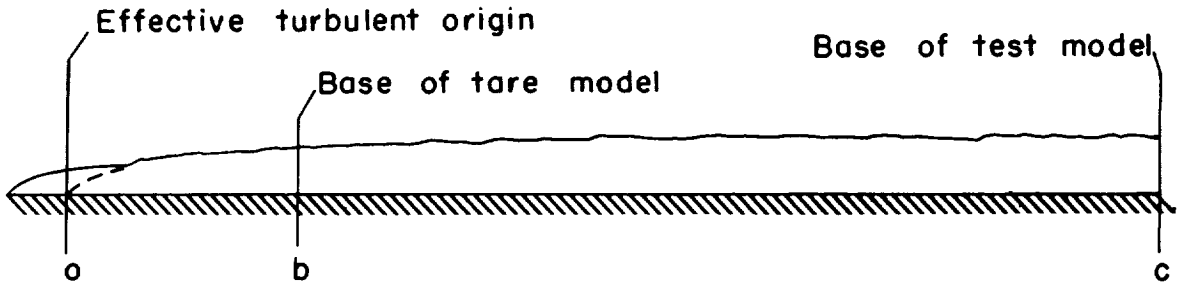

This was determined by subtracting the incompressible skin-friction drag of the area indicated between o and b from the drag of the area indicated between o and c.

$$\left(C_{F_i}\right)_{oc}(S)_{oc} - \left(C_{F_i}\right)_{ob}(S)_{ob} = \left(C_{F_i}\right)_{bc}(S)_{bc}$$

Now $\left(C_{F_i}\right)_{ob}$ and $\left(C_{F_i}\right)_{oc}$ can be calculated from the Kármán-Schoenherr equation if the Reynolds number based on the length ob, R_b and the Reynolds number based on the length oc, R_c are known. The notation R_b, R_c will be used hereafter to designate the Reynolds numbers used in determining the incompressible skin-friction coefficient.

Accuracy

A major effort was expended to control model geometry to insure small scatter in the results. In spite of the best efforts to control model geometry, large scatter was still present. The spread of total-drag results for test and tare models was approximately 5 percent, but the inaccuracy of each individual drag result due to errors in time-distance measurements and air-stream calibration was only about 2 percent, so it is believed that differences in drag did indeed occur due to some unknown cause. This scatter was greatly magnified when test and tare models were combined to obtain skin-friction drag, for the percentage of skin-friction drag to total drag varied from 30 to 60 percent, depending on the test condition. Because of this persistent scatter it was mandatory that a large number of results be obtained at each test condition so that the effect of random scatter due to uncontrolled features of model geometry could be minimized by averaging results. It is believed

that the scatter that remained after all corrections were made was due to the presence of the boundary-layer trips, because these trips could not be reproduced, in all cases, from model to model with the desired precision.

The table below shows the scatter in skin-friction results at each test condition, the number of test results (i.e., with approximately an equal number of test and tare models, the indiscriminate combination of all test and tare models at each test condition), and the symbol that identifies the model geometry in table I.

(1)	(2)	(3)	(4)	(5)	(6)
M_1	$(R_1/x)10^{-6}$	Number of results	RMS deviation from mean, percent	Maximum deviation from mean, percent	Symbol (see table I)
2.81	1.58	12	2.4	+4.0, to -4.2	○
3.82	2.13	12	1.1	+1.8, to -1.8	□
5.63	1.83	24	10.0	+21.2, to -13.3	◇
6.90	2.08	20	8.2	+12.1, to -16.5	□
7.00	3.14	6	9.0	+14.9, to -11.2	■
3.78	2.13	24	7.1	+13.4, to -13.3	▷
3.67	1.99	3	2.9	+3.0, to -3.5	◁

Column (4) in the above table shows the root-mean-square deviation from the arithmetic mean of the data and, statistically, best represents the uncertainty in the skin-friction data. Column (5) shows the maximum deviation from the arithmetic mean and is not nearly representative of the reliability of the measurements. These were included in the table to show the full range of the data even though, in some cases, the result for one combination of test and tare model was approximately 5 percent beyond the range of all other results at that condition.

The three conditions for which the scatter was the least were those where 0.003-inch threads were used as boundary-layer trips. The conditions for which the scatter was appreciable were those where large boundary-layer trips were used. The skin-friction results could be appreciably altered by small changes in trip geometry that could not be detected (on the inner surface of the model, for example). Row (3), where the largest deviations are shown, presented the greatest problem. The 0.006-inch threads used for boundary-layer trips were cut on the circular-arc profile, so that small errors in machining would show up as changes in pressure drag of the trip and of the entire contour as well. These changes in geometry were not accounted for and may possibly explain the magnitude of the deviations.

Because of the large scatter in the initial results at $M_1 = 6.9$, an independent test with the same model geometry at a slightly higher Reynolds number was run at $M_1 = 7.0$. The agreement between the mean results at the two different Reynolds numbers was better than expected, and the difference was well within the root-mean-square deviation of the data.

The more than 300 shadowgraphs of the data models showed turbulent flow over the external surfaces almost as far forward as the boundary-layer trips with no intermittently turbulent and laminar boundary layers. Unfortunately, the boundary layers on the inner surfaces of the cylinders could not be examined, but it is unlikely that these boundary layers would be different than on the outer surfaces because the machining process was the same for both surfaces. The flow over the boundary-layer trips and about 0.1 inch downstream of the trips could not be observed in the shadowgraphs and possibly was intermittently laminar and turbulent. It must be emphasized, however, that this region which could not be observed was restricted to a small section of the tare portion of the test models: therefore, the errors which could be introduced, although not considered, would be small.

TEST RESULTS AND DISCUSSION

Skin-Friction Ratio

The experimentally determined values of skin-friction coefficient in the form C_F/C_{F_i}, hereafter called skin-friction ratio, are plotted as a function of Mach number, M_1, in figure 6. Values of skin-friction coefficient, C_F, are mean values of many measurements at each condition, and values of incompressible skin-friction coefficient, C_{F_i}, were obtained from the Kármán-Schoenherr equation (ref. 14). These data are uncorrected for thickening of the turbulent boundary layer due to the boundary-layer trip. The turbulent origin was determined by assuming that the momentum thickness of the turbulent boundary layer was equal to that of the laminar boundary layer at the transition point (midlength of trip). The values of C_F are unaffected by this assumption, since they were determined experimentally. With the assumption of no initial thickness due to the boundary-layer trip, or so-called natural transition, the resulting values of skin-friction ratio, C_F/C_{F_i}, can be considered as lower limits. Any initial thickness of the boundary layer would mean a higher effective Reynolds number, therefore a lower value of C_{F_i} and, consequently, a higher value of skin-friction ratio, C_F/C_{F_i}.

For comparison, the force data of Chapman and Kester (ref. 1) and Coles (ref. 2) at zero-heat-transfer conditions are also included in the figure. The curve drawn through these points is the mean zero-heat-transfer curve suggested in reference 1. A comparison of the zero-heat-transfer data and the uncorrected data of the present investigation

indicate a strong dependence of skin-friction ratio on wall-temperature ratio, T_w/T_1, at a given Mach number.

Effect of large boundary-layer trips on skin-friction ratio.- Since it was found that large boundary-layer trips were necessary at Mach numbers of 5.6 and 7.0 to promote turbulent flow over the surfaces of the models, it was required that the effect of these large trips on both skin friction and the corresponding incompressible skin friction be investigated.

To investigate experimentally the effect of using a large trip, the skin friction was measured on a model with a boundary-layer trip of 0.006-inch-deep threads and compared to results obtained from a model with 0.003-inch-deep threads at a Mach number of 3.8 where the experimental scatter of skin friction was small. It was found that skin friction was 10 percent lower on the 0.006-inch threaded model than on the 0.003-inch threaded model. The results are plotted in figure 6 as skin-friction ratio. The low value of skin friction was not particularly surprising since the apparent boundary-layer thickness[4] on the 0.006-inch threaded model, as determined from the shadowgraphs, was measurably thicker than that on the 0.003-inch threaded model at corresponding stations along the cylinder. Since the boundary-layer thicknesses were different, the Reynolds numbers were different; consequently, the values of incompressible skin friction were different. In order to determine the effect of the large trip on incompressible skin friction, the following procedure was used. It appeared that there would be a relationship between the trip drag and the thickening of the boundary layer. The trip drag must result in momentum being removed from the air flowing around the model, and part of this momentum will be removed from the boundary-layer air. The amount of increase of the momentum thickness of the turbulent boundary layer is dependent upon the amount of this momentum change confined to the boundary layer. It was necessary, therefore, to make some assumption regarding the amount of momentum removed from the boundary layer as a consequence of the trip drag. As a limiting case, it was assumed that all of the momentum change due to the drag of the trip was confined to the boundary layer. The length of run of turbulent flow necessary to produce the increased momentum thickness was then calculated as explained in Appendix B. The effective turbulent origin was established by this length of run, and a new value of incompressible skin friction was determined. Skin-friction ratio for the 0.006-inch threaded model, corrected in this way for thickening effect of the boundary-layer trip, is plotted in figure 7. The data uncorrected for boundary-layer thickening are also shown in the figure. It can be seen that when only the incompressible skin friction is modified, the results of the 0.003-inch and 0.006-inch threaded models are in reasonable agreement (within the scatter of the experimental results of the 0.006-inch threaded model). The data at Mach numbers of 5.6 and 7.0 were corrected

[4]The actual boundary-layer thicknesses could not be determined due to diffraction and refraction effects.

for boundary-layer thickening effect and are also shown in figure 7. The correction at Mach number of 5.6 was small, but the data at Mach number 7 were raised by about 10 percent, due to the correction in incompressible skin friction.

Since this momentum method involves the assumption as to the amount of momentum change due to the drag of the trip being confined to the boundary layer, it was desired to obtain further evidence as to the reliability of the assumption of total momentum change being confined to the boundary layer. An independent method of determining the effect of large boundary-layer trips was used at a Mach number of 3.8 where apparent boundary-layer thicknesses could be measured from the shadowgraphs. The apparent thicknesses of the turbulent boundary layers of the 0.003-inch and 0.006-inch threaded models were measured and plotted as a function of position from the leading edge. It was then assumed that when the apparent thicknesses of the boundary layers were the same, the actual thicknesses were the same. The additional length of run of turbulent flow necessary to produce the boundary layer observed on the model with 0.006-inch threads was found by moving the x axis until the apparent boundary-layer thicknesses coincided. The effective turbulent origin was then established by this amount of movement of the x axis, and a new value of incompressible skin friction was determined. This value of incompressible skin friction was in excellent agreement with the value determined by assuming total momentum change due to the drag of the trip being confined to the boundary layer. Unfortunately, no check could be made on the corrections used at a Mach number of 7 so the final skin-friction results are presented in figure 7 as bars and are tabulated in table II as a range of possible values, depending upon the amount of correction to incompressible skin friction. The agreement in skin-friction ratio between the 0.003-inch and 0.006-inch threaded models, where the turbulent origins were determined assuming normal "fully developed" turbulent boundary layers, indicates that the characteristics of the turbulent boundary layer over the portion of the model for which skin friction was measured were not significantly affected by the presence of the boundary-layer trips.

Also shown in figure 7 are the zero-heat-transfer data replotted from figure 6. At Mach numbers of 2.8 and 3.8, the skin-friction ratios at $T_w/T_1 = 1.03$ and 1.05 are approximately 35 percent higher than the zero-heat-transfer data. Although no measurements of skin friction have been made at zero-heat-transfer conditions at very high Mach numbers, the data of figure 7 indicate that the same trend of increasing skin-friction ratio with decreasing wall-temperature ratio will persist to a Mach number of 7.

Effect of spin on the present results.- Because figure 7 shows an appreciable effect of wall-temperature ratio on skin-friction ratio, and since the models of the present investigation were spin stabilized, it was essential to determine to what extent these results had been influenced by model spin. The possibility that rotation of the models may

have influenced the boundary layer, thus changing skin-friction drag, was present in spite of the fact that the circumferential velocity was small compared to the forward velocity. For this reason, an investigation was made by firing aerodynamically stable models of the type shown in figure 2(e). It was felt that it was not necessary to repeat the entire investigation, and that one test condition would suffice to demonstrate the effect of spin on the present results. The test condition chosen was $M_o = 3.9$, where experimental scatter was least and trip drag negligible.

Since it was necessary to move the center of gravity of the model as far forward as possible to stabilize the model in flight, it was necessary to use a leading-edge configuration that was fairly blunt; hence, the 15° half-angle was used in lieu of the 10° half-angle of figure 2(a). In addition, since a tare model could not be stabilized in flight, the skin-friction drag was obtained by estimating all of the other drag components: laminar skin-friction drag, base drag, drag due to leading-edge bluntness, wave drag, drag due to angle of attack, and drag due to boundary-layer trip. It was found that at the two other conditions ($M_1 = 2.81$ and $M_1 = 3.82$) where 0.003-inch thread trips were used and the trip drag was negligible, the skin-friction drag could be estimated to within 2 percent of the experimental values if all other drag components were estimated and subtracted from the measured total drag, thereby demonstrating the reliability of this procedure.

The result of this investigation is tabulated in row (7) of table II and is shown in figure 7. It can be concluded that for the spin rates used, the effect of spin on the present results is small, probably within the scatter of the experiment.

The effect of wall-temperature ratio on skin-friction ratio.- The results of figure 7 confirm qualitatively the conclusions of many analyses; namely, those of von Kármán, Monaghan, Tucker, Van Driest, and Clemmow, among many (refs. 3 through 7), that skin-friction ratio increases with decreasing wall-temperature ratio, at a given Mach number and Reynolds number. These analyses differ widely only in the magnitude of this increase, as is shown in figure 8, where skin-friction ratio, C_F/C_{F_i}, is plotted as a function of wall-temperature ratio, T_w/T_1. It is interesting to note that three of these theories (those of von Kármán, Monaghan, and Tucker), predict no effect of Mach number on skin-friction ratio at a given wall-temperature ratio, and that wall-temperature ratio is the controlling parameter. Also indicated in the figure is the point at which wall-temperature ratio is equal to recovery-temperature ratio, $T_w/T_1 = T_r/T_1$, since the difference between the recovery-temperature ratio and the wall-temperature ratio is a measure of the rate of heat transfer through the boundary layer. For consistency and simplicity, values of skin-friction ratio from these theories were calculated with the assumption that $(\mu) \sim (T)^{0.76}$, at a Reynolds number $R_1 = 10^7$. Incompressible skin-friction coefficients were calculated from the Kármán-Schoenherr equation.

The experimental data of figure 7 were included in figure 8 to check the reliability of any one theory to predict skin-friction ratio over a wide range of Mach numbers and heat-transfer conditions. The theories of Van Driest and Clemmow agree well with experimental data at wall-temperature ratios near unity. As wall temperature approaches recovery temperature, these theories overestimate the skin-friction ratio by as much as 20 percent. Although the theories of Tucker and von Kármán were devised for application at zero-heat-transfer conditions ($T_w/T_1 = T_r/T_1$), it is interesting to evaluate C_F/C_{F_i} at conditions of large heat transfer and compare these results with experiment. At a wall-temperature ratio of unity, the theories of Tucker, von Kármán and Monaghan predict a skin-friction ratio of unity, which greatly overestimates skin-friction ratio. At recovery temperatures where experimental data are available, Tucker and Monaghan predict skin-friction ratio reasonably well.

The T' Method For Evaluating Skin Friction

Since no one theory for turbulent flow adequately predicts the effects of both wall-temperature ratio and Mach number on skin-friction ratio, the present authors used the T' method of Rubesin and Johnson (ref. 15) which was developed for laminar flow. Fischer and Norris (ref. 16) in 1949 applied the results of Rubesin and Johnson to correlate heat-transfer data for turbulent flow. Although there was no apparent reason for choosing this laminar-flow method for turbulent flow, Fischer and Norris found that their data when evaluated on both the T' and T_w bases correlated better than when evaluated on a T_1 basis. They indicated that it was inconclusive as to whether the T' method of reference 15 should be used for turbulent flow. Young and Janssen (ref. 17) in 1952 applied the T' method of Rubesin and Johnson to evaluate skin-friction ratio for turbulent flow. They compared skin-friction ratio determined by this method with some zero-heat-transfer data over the limited Mach number range from 1.5 to 2.5. The agreement was good.

With the more complete data now available at zero-heat-transfer conditions and with the results of the present investigation at large rates of heat transfer, it is the purpose of this section to demonstrate the reliability of the T' method in predicting the effect of heat transfer as well as Mach number on skin-friction ratio for turbulent flow.

The T' method of Rubesin and Johnson consisted of finding a temperature, T', at which the density and viscosity for compressible flow must be evaluated if incompressible flow relations for zero heat transfer are to apply. The theoretical results of Crocco-Conforto for laminar flow on a flat plate were used to find this reference temperature, T'.

The following expression was derived:

$$\frac{T'}{T_1} = 1 + 0.032\,M_1^2 + 0.58\left(\frac{T_w}{T_1} - 1\right) \qquad (1)$$

The present authors applied equation (1) and the Kármán-Schoenherr incompressible skin-friction equation for turbulent flow to determine whether equation (1) would predict skin-friction ratio as a function of both Mach number and wall-temperature ratio. Curves of skin-friction ratio as a function of Mach number, calculated from equation (1), are plotted in figure 9, and are compared to zero-heat-transfer data and the primary data at $T_w/T_1 = 1.03$ and $T_w/T_1 = 1.05$ from figure 7. Although equation (1) underestimates the skin-friction ratio at zero heat transfer above a Mach number of 2.5, the shape of the zero-heat-transfer curve is remarkably similar to the trend of the experimental data. Equation (1) also predicts, reasonably well, the effect of large rates of heat transfer on skin-friction ratio.

Encouraged by these results, the authors found new coefficients for equation (1) using the data at a Mach number of 3.82 from the present experiment and from the zero-heat-transfer curve. The following expression was obtained:

$$\frac{T'}{T_1} = 1 + 0.035\,M_1^2 + 0.45\left(\frac{T_w}{T_1} - 1\right) \qquad (2)$$

It is interesting to note that the constants of equation (2) evaluated for turbulent flow are very similar to the constants of equation (1) which were evaluated for laminar flow.

Curves of skin-friction ratio as a function of Mach number were obtained from equation (2) for the temperature conditions of the data of figure 7 and are compared to these data in figure 10. The method of obtaining skin-friction ratio from equation (2) is explained in Appendix C.

The agreement between the predicted values of skin-friction ratio from equation (2) and the experimentally determined values of skin-friction ratio is excellent over the entire range of Mach numbers and wall-temperature conditions for the experimental data of figure 7. It should be emphasized that only two experimental values were used to determine the constants, those at $M_1 = 3.82$. The agreement at the other test conditions therefore represents a test of the method.

Evaluation of skin friction for flight conditions.- The procedure described in Appendix C was used to obtain the curves of figure 11 from equation (2) where skin-friction ratio, C_F/C_{F_i}, is plotted as a function of

Mach number, M_1, over a range of values of wall-temperature ratio, T_w/T_1. The value of $T_1 = 392^\circ$ R, corresponding to the standard isothermal altitude range of 35,000 to 105,000 feet, was used for all calculations. The Sutherland viscosity law was used, with $S_1 = 199^\circ$ R, as given by the National Bureau of Standards (ref. 18). A reference Reynolds number, $R_1 = 10^7$, was used.

There is a significant difference in skin-friction ratio between the zero-heat-transfer curves of figures 10 and 11 at Mach numbers greater than 4. The zero-heat-transfer curve of figure 10 was calculated for wind-tunnel-test conditions assuming a constant wind-tunnel reservoir temperature, therefore, T_1 reduced rapidly at high Mach numbers. The curves of figure 11 are more nearly representative of flight conditions at high altitudes.

Comparison of the T' method with theory and experiment at subsonic speeds.- The curves of figure 11 predict very large changes in skin-friction ratio with changes in wall-temperature ratio at the low Mach numbers, particularly at subsonic speeds. Because of the lack of suitable experimental data on flat plates with large rates of heat transfer, the predictions of the T' method were compared with experimental data on turbulent flow in smooth pipes at subsonic speeds. Since experimental skin-friction results at large rates of heat transfer in smooth pipes were very meager, heat-transfer data were also used in the form of Stanton number ratios, $St/St_{(T_w = T_1)}$. It has been demonstrated by Colburn (ref. 19) that Stanton number is proportional to skin friction or that Stanton number ratio is equivalent to skin-friction ratio. In figure 12, skin-friction ratio as determined by use of equation (2) at $M = 0$ is compared to experimental and theoretical results of skin-friction ratio and Stanton number ratio as a function of wall-temperature ratio for turbulent flow in smooth pipes. The Reynolds number based on pipe diameter, R_D, of the experimental data is 10^5. Reynolds number based on length of run of turbulent flow on a flat plate, R_1, was calculated to be 2.6×10^6 for $R_D = 10^5$, for a boundary-layer thickness equal to the radius of the pipe. This Reynolds number, $R_1 = 2.6 \times 10^6$ was used in equation (2) to obtain results for comparison with the data.

Colburn (ref. 19) and McAdams (ref. 20) have shown that if viscosity is evaluated at a film temperature (equivalent in purpose to the present T'), $T_f = 1/2\ T_w + 1/2\ T_1$, the skin-friction equations for zero heat transfer in smooth pipes could be applied to flow with heat transfer. The Drew, Koo, and McAdams equation (ref. 19),

$$C_F = 0.0014 + 0.125\ R_D^{-0.32}$$

and the Kármán-Nikuradse equation (ref. 21),

$$\frac{1}{\sqrt{4C_F}} = 2 \log_{10}(R_D\sqrt{4C_F}) - 0.8$$

were both evaluated at the film temperature, as defined above. The Drew, Koo, and McAdams equation, and the Kármán-Nikuradse equation gave results at $R_D = 10^5$ that differed very slightly from the results of equation (2). Skin-friction ratio, as determined from equation (2) agreed well with the experimental skin-friction results of reference 21 and was slightly higher over the entire range of wall-temperature ratios when compared to the heat-transfer results of references 21 and 22. It appears probable that equation (2) can be used to predict skin-friction ratio at subsonic Mach numbers.

Comparison of the T' method with experimental results of reference 23.- For Mach numbers above 4.5 there is very little experimental data available against which to check the T' method other than the data already presented in the preceding sections of this paper. In fact, the only additional data in this Mach number range known to the authors are the data of reference 23. Unfortunately, these data are not for flat-plate conditions, being a set of measurements of the turbulent boundary layer on a nozzle wall at Mach numbers of 5.0, 6.8, and 7.7. The values of local skin-friction coefficients and the corresponding values of local incompressible skin-friction coefficients were based, in reference 23, on the same R_θ (Reynolds number based on momentum thickness). It was therefore necessary for comparison with the present results to re-evaluate the local incompressible skin-friction coefficients so that the values of local skin-friction coefficients and the corresponding values of local incompressible skin-friction coefficients, c_{f_i}, were based on the same R_1 (Reynolds number based on length of run of turbulent flow on a flat plate). The resulting expression for local incompressible skin-friction coefficient based on R_1 and derived from the Kármán-Schoenherr equation is

$$c_{f_i} = \frac{0.0293}{\log_{10}\frac{2R_\theta}{(c_f/c_{f_i})_{R_\theta}}\left(\frac{1}{2}\log_{10}\frac{2R_\theta}{(c_f/c_{f_i})_{R_\theta}} + 0.4343\right)}$$

where R_θ and $(c_f/c_{f_i})_{R_\theta}$ are the values given in reference 23.

The experimental results in the ratio of skin friction to incompressible skin friction, c_f/c_{f_i}, are shown in figure 13 and are compared with skin-friction ratio as determined by use of equation (2) for the temperature conditions of the experiment. It can be seen that although the data show no definite trends of the effect of heat transfer on skin-friction ratio, the level of the data is in fair agreement with the results from the T' method. The T' method predicts a large change in skin-friction ratio between zero-heat-transfer conditions and conditions where the wall-temperature ratio is unity; however, for the heat-transfer conditions of the experiment, the T' method predicts a relatively small change in skin-friction ratio. The measured changes in skin-friction ratio are, in general, of the same order of magnitude to

be expected from the T' method; however, in some cases, the changes are of opposite sign.

Predicted effect of Reynolds number on skin-friction ratio.- The predicted effect of Reynolds number on skin-friction ratio was investigated by evaluating equation (2) at standard isothermal altitude conditions, and using the procedure described previously. The effect of Reynolds number on skin-friction ratio at Mach numbers of 2 and 8, at $T_w = T_1$ and $T_w = T_r$, is shown in figure 14. It can be seen that at a Mach number of 2, over the wide Reynolds number range from 10^6 to 10^8, that the predicted Reynolds number effect on skin-friction ratio is small. In fact, the magnitude of this predicted effect over the Reynolds number range from 3×10^6 to 30×10^6 is so small, less than 2 percent, that it would be difficult to confirm experimentally. This prediction is consistent with the results of Chapman and Kester (ref. 1) where no Reynolds number effect on skin-friction ratio was detected at Mach numbers up to 3.6. At a Mach number of 8, however, the predicted effect of Reynolds number on skin-friction ratio over the Reynolds number range from 3×10^6 to 30×10^6 is the order of 5 to 10 percent. Over the Reynolds number range from 10^6 to 10^8, the predicted effect is the order of 10 to 25 percent. This analysis was made to caution the reader about the validity of the assumption that skin-friction ratio is invariant with Reynolds number. Since the Reynolds numbers encountered in high-speed, high-altitude flight can be expected to be in the order of several hundred millions, the application of equation (2) with the assumption of no Reynolds number effect on skin-friction ratio may produce serious discrepancies.

CONCLUSIONS

Experimental measurements of skin friction of the turbulent boundary layer have been made on free-flying models at high supersonic speeds. The results of this investigation can be summarized as follows:

1. The effect of wall-temperature ratio on skin-friction ratio is large, an increase of the order of 35 percent at Mach numbers of 2.81 and 3.82, when free-flight data of this experiment are compared with zero-heat-transfer skin friction data.

2. Although skin-friction measurements at conditions of zero heat transfer are not available at Mach numbers as high as 7, the results of this investigation indicate that the same trend of increasing skin-friction ratio with decreasing wall-temperature ratio will persist at very high Mach numbers.

3. The T' method of Rubesin and Johnson for laminar boundary layers has been used to evaluate skin friction of the turbulent boundary layer. By use of slightly modified equations with experimentally

determined constants, computed values of skin-friction ratio agree well with measured values over a wide range of Mach numbers and wall-temperature ratios.

Ames Aeronautical Laboratory
National Advisory Committee for Aeronautics
Moffett Field, Calif., Dec. 8, 1954

APPENDIX A

ESTIMATION OF SURFACE TEMPERATURE

In order to determine the heat-transfer conditions of the present investigation, it was necessary to evaluate the wall-temperature ratio, T_w/T_1. The determination of T_w/T_1 was a transient-condition problem due to the short flight time of the models, the order of 0.01 second. Neglecting axial heat flow, the solution of this problem is given in paragraph 41, equation (2) of reference 24 and is shown below in the nomenclature of this paper.

$$\frac{T - T_i}{T_r - T_i} = 1 - \sum_{n=1}^{\infty} \cdot \frac{2\,\frac{y_1 H}{k_m} \cos\left(\frac{\beta_n y}{y_1}\right)}{\left[\beta_n^2 + \frac{y_1 H}{k_m} + \left(\frac{y_1 H}{k_m}\right)^2\right] \cos \beta_n} e^{-\left(\frac{\beta_n}{y_1}\right)^2 \alpha t} \qquad (A1)$$

where

H average heat-transfer coefficient

k_m thermal conductivity of the model material

t time

T absolute temperature

T_i initial temperature of the model

T_r recovery temperature

T_w temperature at $y = y_1$

y normal distance from the midplane of the model wall

y_1 half-wall thickness

α thermal diffusivity of the model material

β_n positive roots of $\beta \tan \beta = \frac{y_1 H}{k_m}$ (values tabulated in Appendix IV, ref. 24)

For the present purposes, the series converges with one term. In addition, the values of β_1 were very small so $\tan \beta \approx \beta$ and $\beta_1 = \sqrt{\frac{y_1 H}{k_m}}$;

therefore, at $y = y_1$ equation (A1) simplifies to

$$\frac{T_w - T_i}{T_r - T_i} = 1 - \frac{2}{2 + \frac{y_1 H}{k_m}} e^{-\frac{\alpha H}{y_1 k_m} t} \tag{A2}$$

The values of T_w/T_1 listed in this report are the mean values over the portion of the test models for which skin friction was measured. The maximum variation of T_w over this portion of the models was 3° F which resulted in a maximum variation of T_w/T_1 of only 0.02. Axial heat flow, which was not considered, would have a negligible effect on T_w in this region.

APPENDIX B

DETERMINATION OF TURBULENT ORIGIN

It was assumed that in the presence of small boundary-layer trips, the effective point of origin of turbulent flow could be determined by the following method:

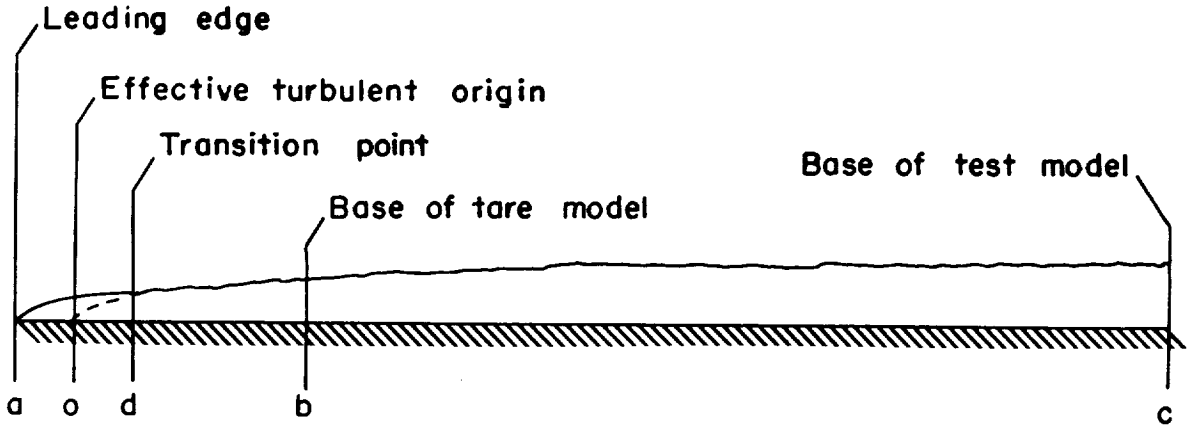

Assume the momentum thickness of the turbulent boundary layer, θ_T, is equal to the momentum thickness of the laminar boundary layer, θ_L, at the transition point, d.

$$\theta_{L_d} = \theta_{T_d}$$

Substitute

$$\theta = \frac{C_F x}{2}$$

then

$$\left(C_{F_L} x\right)_{ad} = \left(C_F x\right)_{od}$$

$$\left(C_{F_L} x\right)_{ad} = \left[\left(C_F / C_{F_i}\right) C_{F_i} x\right]_{od}$$

$$\frac{\left(C_{F_L} x\right)_{ad}}{\left(C_{F_i} x\right)_{od}} = \left(C_F / C_{F_i}\right)_{od} \tag{B1}$$

Now for the present investigation, the experimentally determined C_F is based on the area included between the indicated points b and c. The incompressible skin-friction coefficient based on the same area is

$$\left(C_{F_i}\right)_{bc} = \frac{\left(C_{F_i}x\right)_{oc} - \left(C_{F_i}x\right)_{ob}}{(x)_{bc}}$$

so

$$\left(\frac{C_F}{C_{F_i}}\right)_{bc} = \frac{(C_Fx)_{bc}}{\left(C_{F_i}x\right)_{oc} - \left(C_{F_i}x\right)_{ob}} \tag{B2}$$

If it is assumed that C_F/C_{F_i} is invariant with Reynolds number, then $\left(C_F/C_{F_i}\right)_{bc} = \left(C_F/C_{F_i}\right)_{od}$ and equations (B1) and (B2) can be combined.

$$\frac{(C_Fx)_{bc}}{\left(C_{F_i}x\right)_{oc} - \left(C_{F_i}x\right)_{ob}} = \frac{\left(C_{F_L}x\right)_{ad}}{\left(C_{F_i}x\right)_{od}} \tag{B3}$$

For each test condition, the position o can be found which will satisfy this equality. If M_1 and T_w/T_1 are known, the value of C_{F_L} can be obtained from reference 25; if the Reynolds number per inch, R_1/x, is known, the values of C_{F_i} can be calculated from the Kármán-Schoenherr equation. The value of C_F was determined experimentally. The left side of equation (B3), $\left(C_F/C_{F_i}\right)_{bc}$, which includes the measured value of C_F, is not strongly dependent on the position of the effective turbulent origin; consequently, $\left(C_F/C_{F_i}\right)_{bc}$ as a function of the position o is nearly a horizontal line. The right side of equation (B3), however, is very strongly dependent on the position o and intersects $\left(C_F/C_{F_i}\right)_{bc}$ almost perpendicularly. The position of the effective turbulent origin is therefore sharply defined.

The assumption that C_F/C_{F_i} is invariant with Reynolds number seems to be justified because existing data indicate that C_F/C_{F_i} is very

nearly independent of Reynolds number (ref. 1). According to the T' method of this report, it appears that there may be some dependence of C_F/C_{F_i} on Reynolds number; however, for the present purposes, the effect of Reynolds number on C_F/C_{F_i} would be small (the order of 2 percent) because of the limited range of Reynolds number variation.

In the presence of large boundary-layer trips, the assumption of equal laminar and turbulent momentum thicknesses at the transition point is unjustified; therefore, the following method was used to determine the position of the effective turbulent origin:

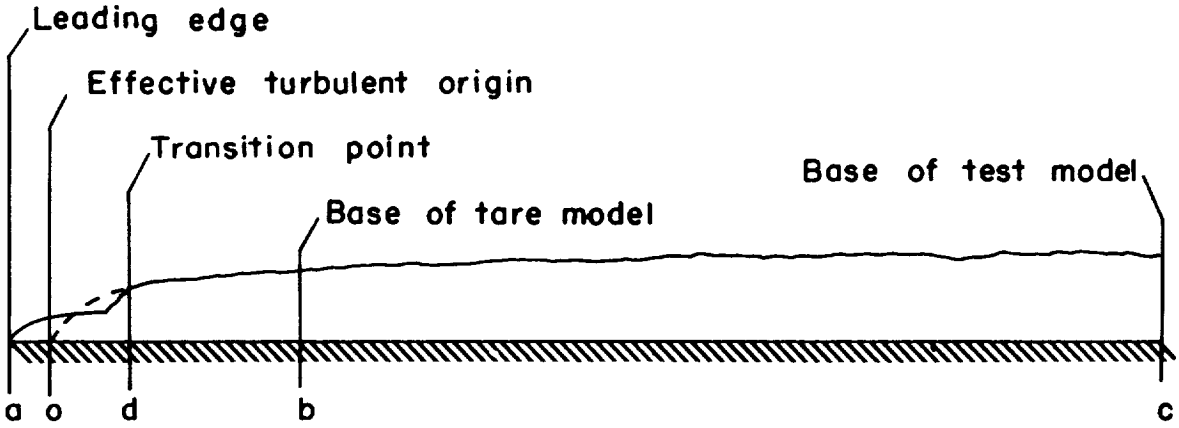

At the transition point, d, the momentum thickness of the turbulent boundary layer is equal to the momentum thickness of the laminar boundary layer plus an increment due to the presence of the trip,

$$\theta_{T_d} = \frac{1}{2}(C_F x)_{od} = \frac{1}{2}\left(C_{F_L} x\right)_{ad} + \Delta\theta \qquad (B4)$$

If $\Delta\theta$ is related to the drag of the trip, it is proportional to only that part of the trip drag which results in removing momentum from the boundary layer. The term "trip drag" used hereafter refers to the percentage of trip drag which results in removing momentum from the boundary layer. The momentum loss in the boundary layer up to the point d is equal to the friction drag of the laminar boundary layer plus the trip drag.

$$C_{F_L}\, q\, 2\pi r x + C_{d_t}\, q\, 2\pi r x = \int_o^\delta 2\pi r \rho u(u_1 - u)\,dy$$

$$\frac{1}{2}\left(C_{F_L} x\right)_{ad} + \frac{1}{2}\left(C_{d_t} x\right)_{ad} = \int_o^\delta \left(\frac{\rho}{\rho_1}\right)\left(\frac{u}{u_1}\right)\left(1 - \frac{u}{u_1}\right)dy = \theta_{T_d} \qquad (B5)$$

Combining equations (B4) and (B5) produces

$$\Delta\theta = \frac{1}{2}\left(C_{d_t}x\right)_{ad} \tag{B6}$$

To relate this to some known quantity, such as the total drag, the trip drag is expressed as a percentage of total drag

$$\left(C_{d_t}x\right)_{ad} = A(C_Dx)_{ac} \tag{B7}$$

Substitute equations (B6) and (B7) into (B4)

$$(C_Fx)_{od} = \left(C_{F_L}x\right)_{ad} + A(C_Dx)_{ac}$$

$$\left[\left(C_F/C_{F_i}\right)C_{F_i}x\right]_{od} = \left(C_{F_L}x\right)_{ad} + A(C_Dx)_{ac}$$

$$\left(C_F/C_{F_i}\right)_{od} = \frac{\left(C_{F_L}x\right)_{ad} + A(C_Dx)_{ac}}{\left(C_{F_i}x\right)_{od}} \tag{B8}$$

Assume C_F/C_{F_i} is invariant with Reynolds number and combine equations (B8) and (B2).

$$\frac{(C_Fx)_{bc}}{\left(C_{F_i}x\right)_{oc} - \left(C_{F_i}x\right)_{ob}} = \frac{\left(C_{F_L}x\right)_{ad} + A(C_Dx)_{ac}}{\left(C_{F_i}x\right)_{od}} \tag{B9}$$

To determine the position o which will satisfy this equality, it is necessary to make some assumption regarding A. For the present investigation, it was assumed that all the momentum change due to the drag of the trip was confined to the boundary layer, and the trip drag was calculated by subtracting the estimated components of drag from the measured total drag of the test models. Note that when the trip drag is negligible, $A = 0$ and equation (B9) reduces to equation (B3). The same method was employed to solve equation (B9) as was used for equation (B3).

APPENDIX C

PROCEDURE FOR DETERMINING SKIN-FRICTION RATIO BY THE T' METHOD

In order to evaluate skin-friction ratio, C_F/C_{F_i}, for any Mach number, M_1, at any wall-temperature ratio, T_W/T_1, for a given Reynolds number, R_1, by the T' method using equation (2) and the Kármán-Schoenherr incompressible flow equation, the following procedure should be followed:

1. Evaluate $\frac{T'}{T_1}$ from equation (2),

$$\frac{T'}{T_1} = 1 + 0.035\ M_1^2 + 0.45\left(\frac{T_W}{T_1} - 1\right)$$

2. Evaluate R' from the following relationship:

$$\frac{R'}{R_1} = \left(\frac{\rho'}{\rho_1}\right)\left(\frac{\mu_1}{\mu'}\right)$$

but considering constant pressure through the boundary layer, $\frac{\rho'}{\rho_1} = \frac{T_1}{T'}$; therefore,

$$\frac{R'}{R_1} = \frac{1}{\left(\frac{T'}{T_1}\right)\left(\frac{\mu'}{\mu_1}\right)} \tag{C1}$$

The ratio, (μ'/μ_1), can be determined from the Sutherland equation,

$$\frac{\mu'}{\mu_1} = \left(\frac{T'}{T_1}\right)^{1.5}\left(\frac{T_1 + S_1}{T' + S_1}\right)$$

($S_1 = 216^\circ$ R and Reynolds number, $R_1 = 10^7$, were used to evaluate the curves of fig. 10).

3. Evaluate C_F' from the Kármán-Schoenherr equation in the form

$$\frac{0.242}{\sqrt{C_F'}} = \log_{10}(C_F'R') \tag{C2}$$

using R' from equation (C1).

4. Evaluate C_F from the relationship:

$$\frac{C_F'}{C_F} = \frac{\rho_1}{\rho'}$$

but since $\frac{\rho_1}{\rho'} = \frac{T'}{T_1}$

$$\frac{C_F'}{C_F} = \frac{T'}{T_1} \tag{C3}$$

using C_F' from equation (C2) and $\frac{T'}{T_1}$ from equation (2) as determined previously.

5. Evaluate C_{F_i} from the Kármán-Schoenherr equation in the form

$$\frac{0.242}{\sqrt{C_{F_i}}} = \log_{10}(C_{F_i}R_1) \tag{C4}$$

It should be pointed out that the evaluation of skin-friction ratio by use of equation (2) can be simplified if the Prandtl-Schlicting relationship,

$$C_F = \frac{0.46}{(\log_{10}R)^{2.6}} \tag{C5}$$

for incompressible flow is used instead of the Kármán-Schoenherr equation.

When equation (C5) is combined with equation (2), the resulting equation for the evaluation of C_F/C_{F_i} is:

$$\frac{C_F}{C_{F_i}} = \frac{1}{T'/T_1}\left[\frac{\log_{10}R_1}{\log_{10}\frac{R_1}{(T'/T_1)(\mu'/\mu_1)}}\right]^{2.6} \tag{C6}$$

where C_F/C_{F_i} can be evaluated directly.

The authors chose to use the Kármán-Schoenherr equation throughout this paper, although the Prandtl-Schlicting equation fits the existing low-speed skin-friction data equally well. The authors wished to be consistent with other authors who have used the Kármán-Schoenherr equation.

REFERENCES

1. Chapman, Dean R., and Kester, Robert H.: Turbulent Boundary-Layer and Skin-Friction Measurements in Axial Flow Along Cylinders at Mach Numbers Between 0.5 and 3.6. NACA TN 3097, 1954.

2. Coles, D.: Measurements in the Boundary Layer on a Smooth Flat Plate in Supersonic Flow. PH. D. Thesis, Calif. Inst. Tech., 1953.

3. von Kármán, Th.: The Problems of Resistance in Compressible Fluids. GALCIT Pub. No. 75, 1936 (From R. Accad. D' Italia, 1936).

4. Monaghan, R. J.: A Review and Assessment of Various Formulae for Turbulent Skin Friction in Compressible Flow. British RAE TN No. Aero. 2182, 1952.

5. Tucker, Maurice: Approximate Calculation of Turbulent Boundary-Layer Development in Compressible Flow. NACA TN 2337, 1951.

6. Van Driest, E. R.: Turbulent Boundary Layer Flow in Compressible Fluids. Jour. Aero. Sci., vol. 18, no. 3, Mar. 1951, p. 145.

7. Clemmow, D. M.: The Turbulent Boundary Layer Flow of a Compressible Fluid Along a Flat Plate. British, Rep. No. 50/6, Director of Guided Weapons Research and Development, Aug. 1950.

8. Seiff, Alvin: Examination of the Existing Data on the Heat Transfer of Turbulent Boundary Layers at Supersonic Speeds from the Point of View of Reynolds Analogy. NACA TN 3284, 1954.

9. Seiff, Alvin, James, Carlton S., Canning, Thomas N., and Boissevain, Alfred G.: The Ames Supersonic Free-Flight Wind Tunnel. NACA RM A52A24, 1952.

10. Thielsch, Helmut: Visual and Optical Evaluation of Metal Surfaces. Metal Finishing, May 1951, pp. 54-61.

11. Eggers, A. J., Jr., Syvertson, Clarence A., and Kraus, Samuel: A Study of Inviscid Flow About Airfoils at High Supersonic Speeds. NACA Rep. 1123, 1953.

12. Chapman, Dean R., Wimbrow, William R., and Kester, Robert H.: Experimental Investigation of Base Pressure on Blunt-Trailing-Edge Wings at Supersonic Velocities. NACA Rep. 1109, 1952.

13. Staff of the Ames 1- by 3-foot Supersonic Wind-Tunnel Section: Notes and Tables for Use in the Analysis of Supersonic Flow. NACA TN 1428, 1947.

14. Schoenherr, Karl E.: Resistance of Flat Surfaces Moving Through a Fluid. Soc. of Naval Arch. and Marine Engrs. Trans., vol. 40, 1932, pp. 279-313.

15. Rubesin, Morris W., and Johnson, H. A.: A Critical Review of Skin-Friction and Heat-Transfer Solutions of the Laminar Boundary Layer of a Flat Plate. ASME Trans., vol. 71, no. 4, May 1949, p. 383.

16. Fischer, W. W., and Norris, R. H.: Supersonic Convective Heat-Transfer Correlation from Skin-Temperature Measurements on a V-2 Rocket in Flight. ASME Trans., vol. 71, no. 5, July 1949, pp. 457-470.

17. Young, George B. W., and Jassen, Earl: The Compressible Boundary Layer. Jour. Aero. Sci., vol. 19, no. 4, Apr. 1952, pp. 229-236.

18. Morey, F. C.: The NBS-NACA Tables of Thermal Properties of Gases. National Bureau of Standards, Table 2.39, Dry Air, Dec. 1950.

19. Colburn, Allan P.: A Method of Correlating Forced Convection Heat Transfer Data and a Comparison with Fluid Friction. American Inst. of Chem. Engrs. Trans., vol. XXIX, 1933, pp. 174-210.

20. McAdams, William H.: Heat Transmission, Second ed., McGraw-Hill, 1942.

21. Loudermilk, Warren H., and Grele, Milton D.: Heat Transfer From High-Temperature Surfaces to Fluids. II - Correlation of Heat-Transfer and Friction Data for Air Flowing in Inconel Tube with Rounded Entrance. NACA RM E8L03, 1949.

22. Desmon, L. G., and Sams, E. W.: Correlation of Forced-Convection Heat-Transfer Data for Air Flowing in Smooth Platinum Tube with Long-Approach Entrance at High Surface and Inlet-Air Temperatures. NACA RM E50H23, 1950.

23. Lobb, Kenneth R., Winkler, Eva M., and Persh, Jerome: Experimental Investigation of Turbulent Boundary Layers in Hypersonic Flow. I.A.S. Preprint No. 452, 1954.

24. Carslaw, H. S., and Jaeger, J. C.: Conduction of Heat in Solids. Oxford Univ. Press, 1948, pp. 93-102, 377.

25. Van Driest, E. R.: Investigation of the Laminar Boundary Layer in Compressible Fluids Using the Crocco Method. NACA TN 2597, 1952.

TABLE I.- TEST CONDITIONS AND MODEL CONFIGURATIONS

(1)	(2)	(3)	(4)	(5)	(6)	(7)	(8)	(9)	(10)
M_o	$\frac{R_o}{x}10^{-6}$, per in.	M_1	$\frac{R_1}{x}10^{-6}$, per in.	Gun bore	l, in.	Figure number for nose profile and boundary layer trip	$\frac{T_w}{T_1}$	$\frac{T_r}{T_1}$	Symbol
2.84	1.61	2.81	1.58	Rifled	2.0	2(a)	1.03	2.40	○
3.88	2.24	3.82	2.13	Rifled	2.0	2(a)	1.05	3.60	□
7.09	3.64	5.63	1.83	Rifled	2.5	2(b)	1.29	6.64	◇
7.31	2.52	6.90	2.08	Rifled	2.0	2(c)	1.70	9.47	▯
7.41	3.82	7.00	3.14	Rifled	2.0	2(c)	1.75	9.72	■
3.86	2.23	3.78	2.13	Rifled	2.0	2(d)	1.05	3.54	▷
3.80	2.23	3.67	1.99	Smooth	2.0	2(e)	1.05	3.40	◁

NACA

TABLE II.- FINAL RESULTS

M_1	$\frac{T_w}{T_1}$	$\frac{R_1}{x}10^{-6}$	R_b10^{-6}	R_c10^{-6}	C_F	$\frac{C_F}{C_{F_i}}$	Symbol (see table I)
2.81	1.03	1.58	0.63	3.00	0.00284	0.867	○
3.82	1.05	2.13	.88	4.07	.00227	.730	□
5.63	1.29	1.83	1.05	4.71	.00170	.562	◇
6.90	1.70	2.08	1.03 to 2.97	4.06 to 6.09	.00125	.404 to .451	▯
7.00	1.75	3.14	1.35 to 5.21	6.06 to 9.92	.00115	.395 to .446	■
3.78	1.05	2.13	1.75	4.94	.00204	.694	▷
3.67	1.05	1.99	.20	3.78	.00240	.724	◁

NACA

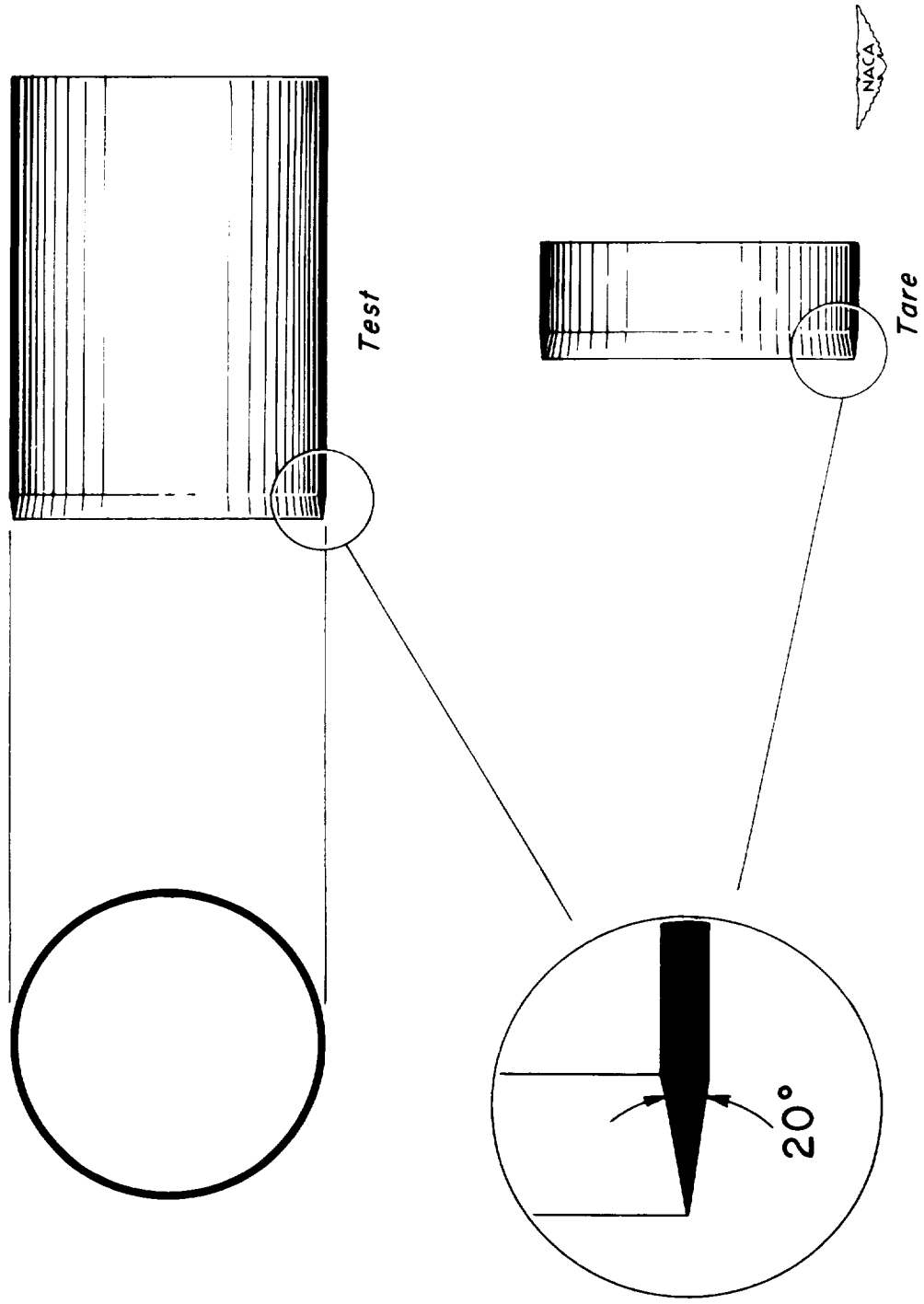

Figure 1.- Typical models.

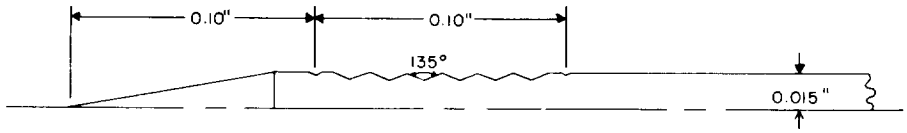

(a) 10° half-angle wedge, 6 threads 0.003 inch deep

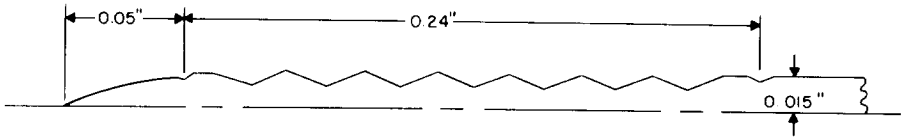

(b) Circular arc with 20° tangent angle, 7 threads 0.006 inch deep

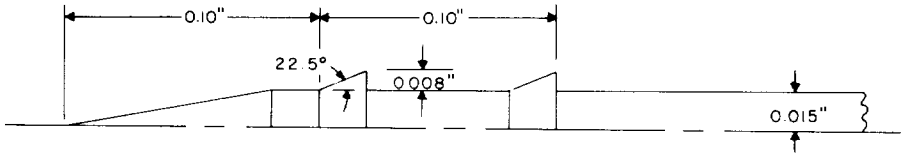

(c) 10° half-angle wedge, 2 annular rings 0.008 inch high

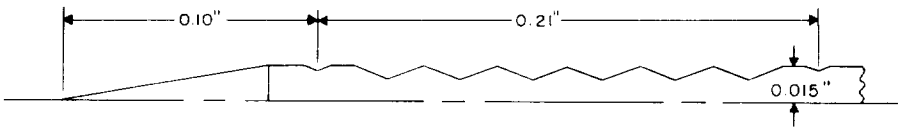

(d) 10° half-angle wedge, 6 threads 0.006 inch deep

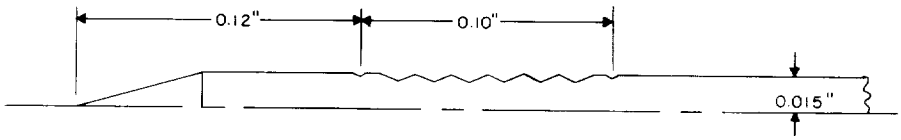

(e) 15° half-angle wedge, 6 threads 0.003 inch deep

Figure 2.- Nose profiles and boundary-layer trips.

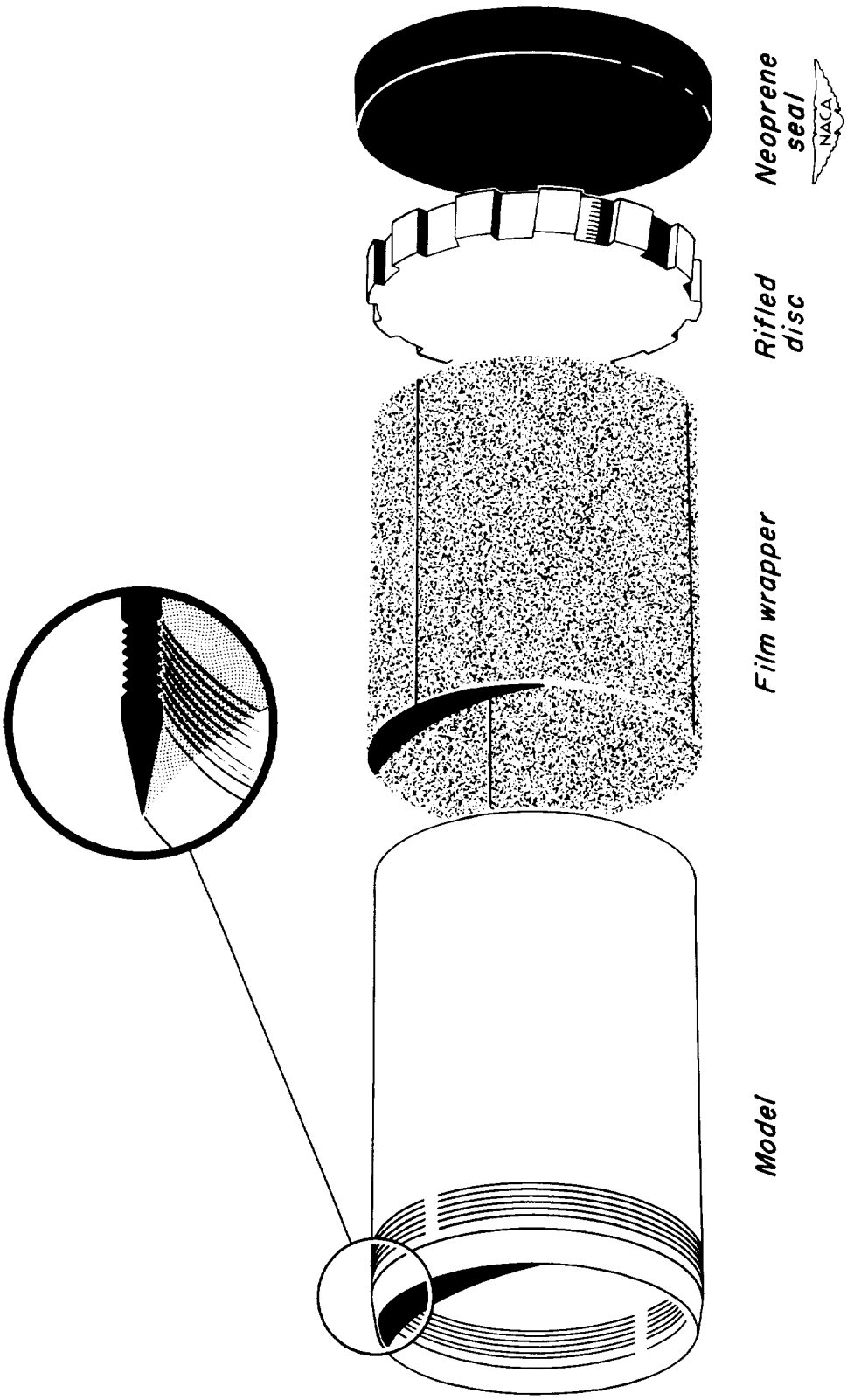

Figure 3.- Test model assembly, exploded view.

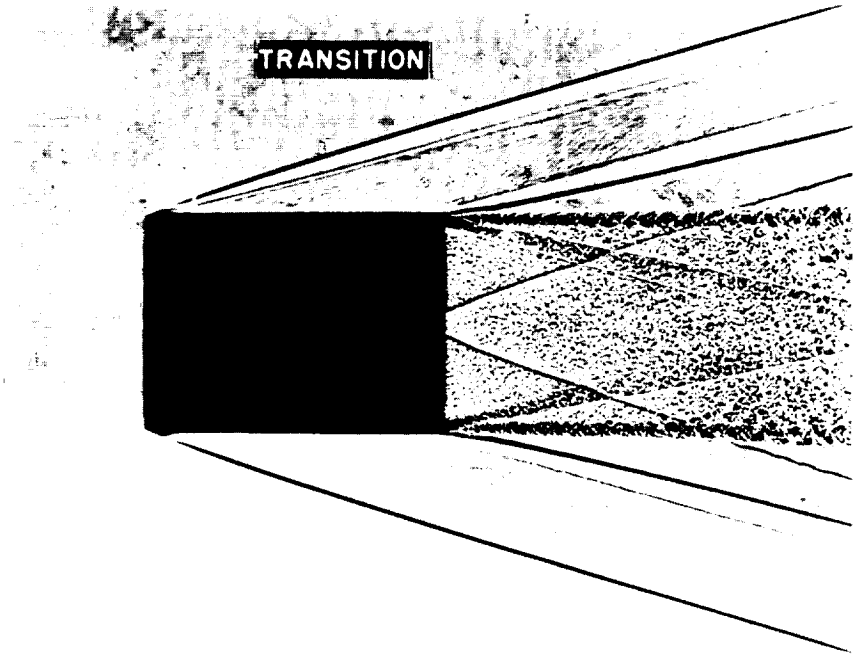

(a) 10° half-angle wedge, 6 threads 0.003 inch deep

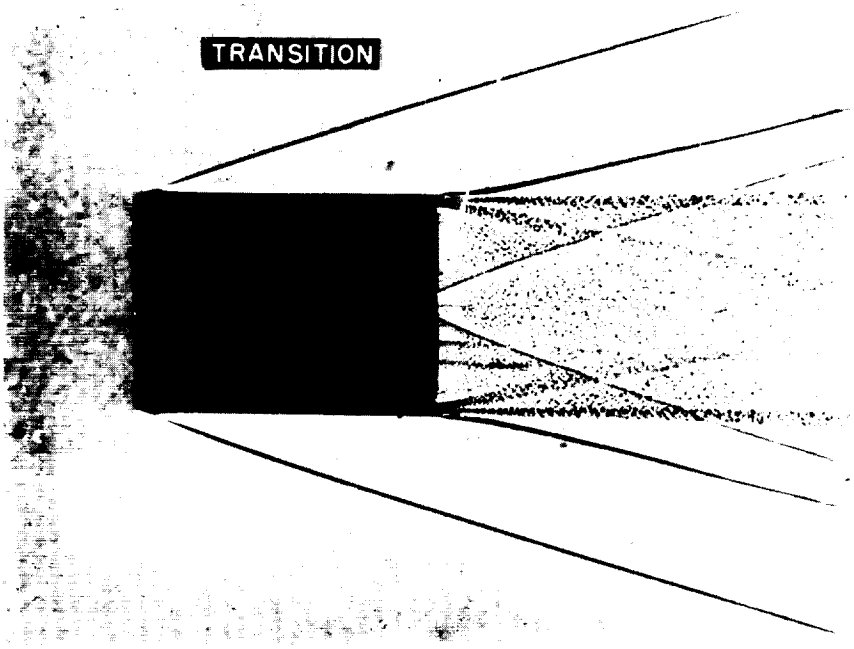

(b) 10° half-angle wedge, 6 threads 0.001 inch deep

Figure 4.- Shadowgraphs of test models at M_o = 3.90.

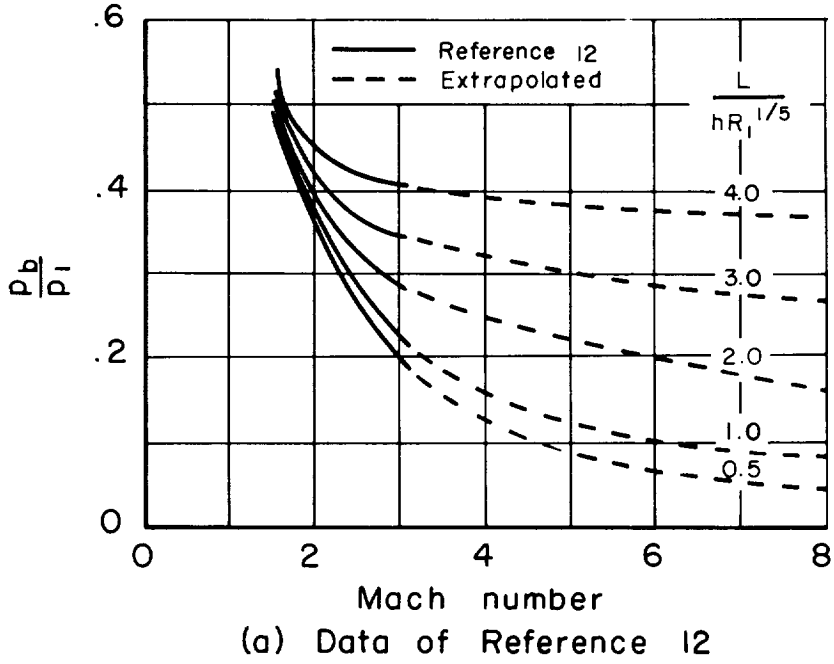

(a) Data of Reference 12

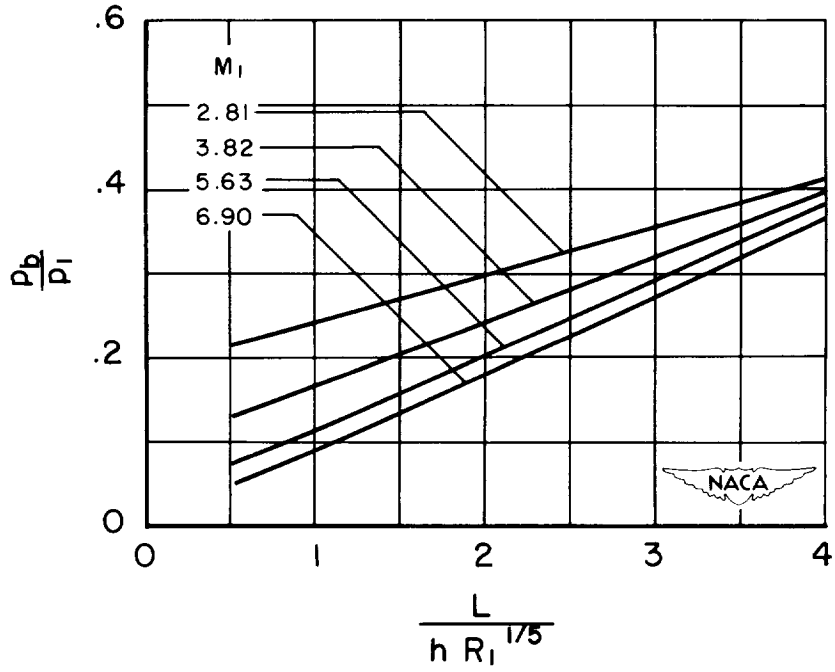

(b) Cross plot of 5(a)

Figure 5.- The effect of Mach number on base pressure for two-dimensional wings in turbulent flow.

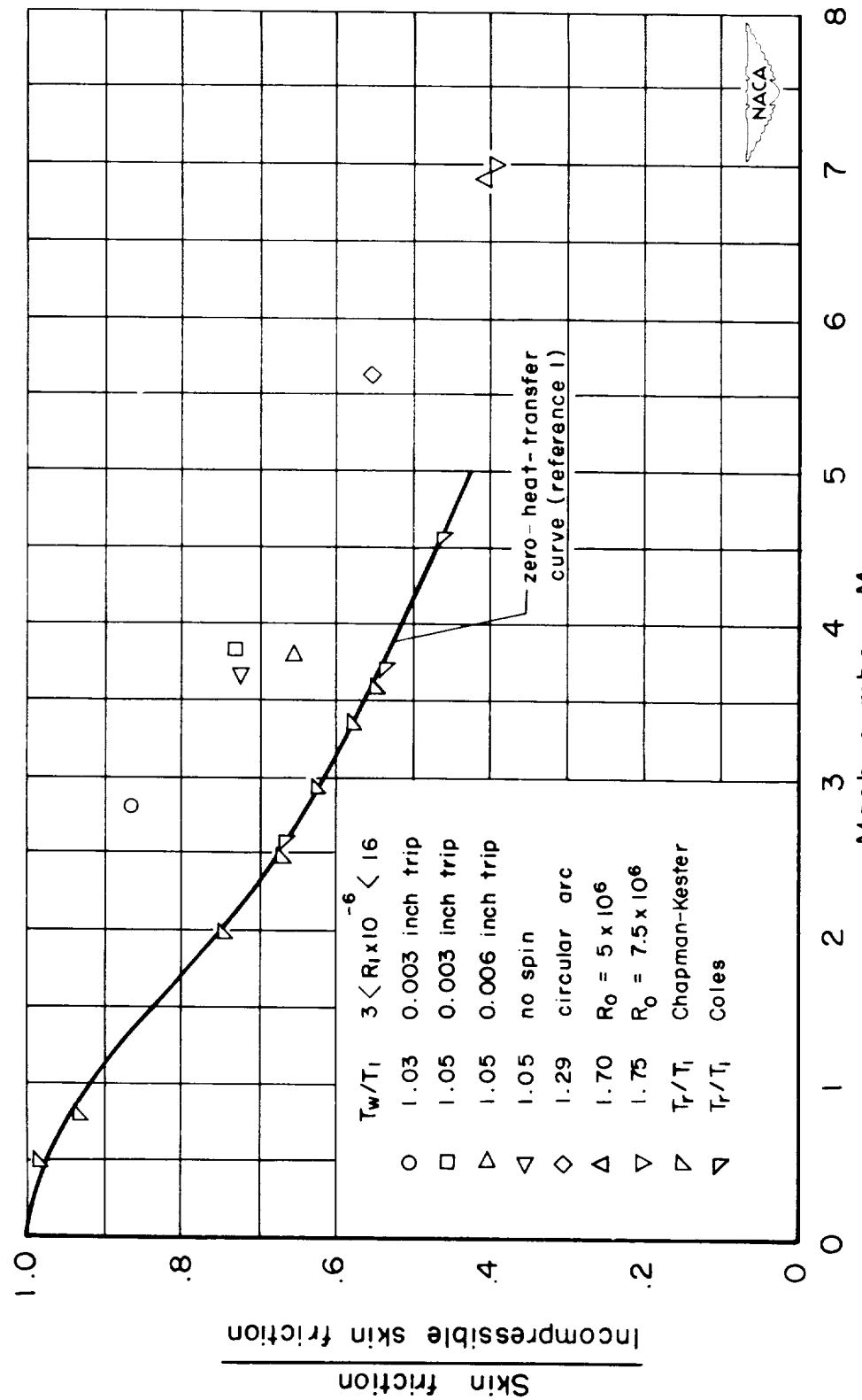

Figure 6.- Effect of Mach number on skin-friction ratio with various wall-temperature ratios, with present data uncorrected for boundary-layer thickening at the trip.

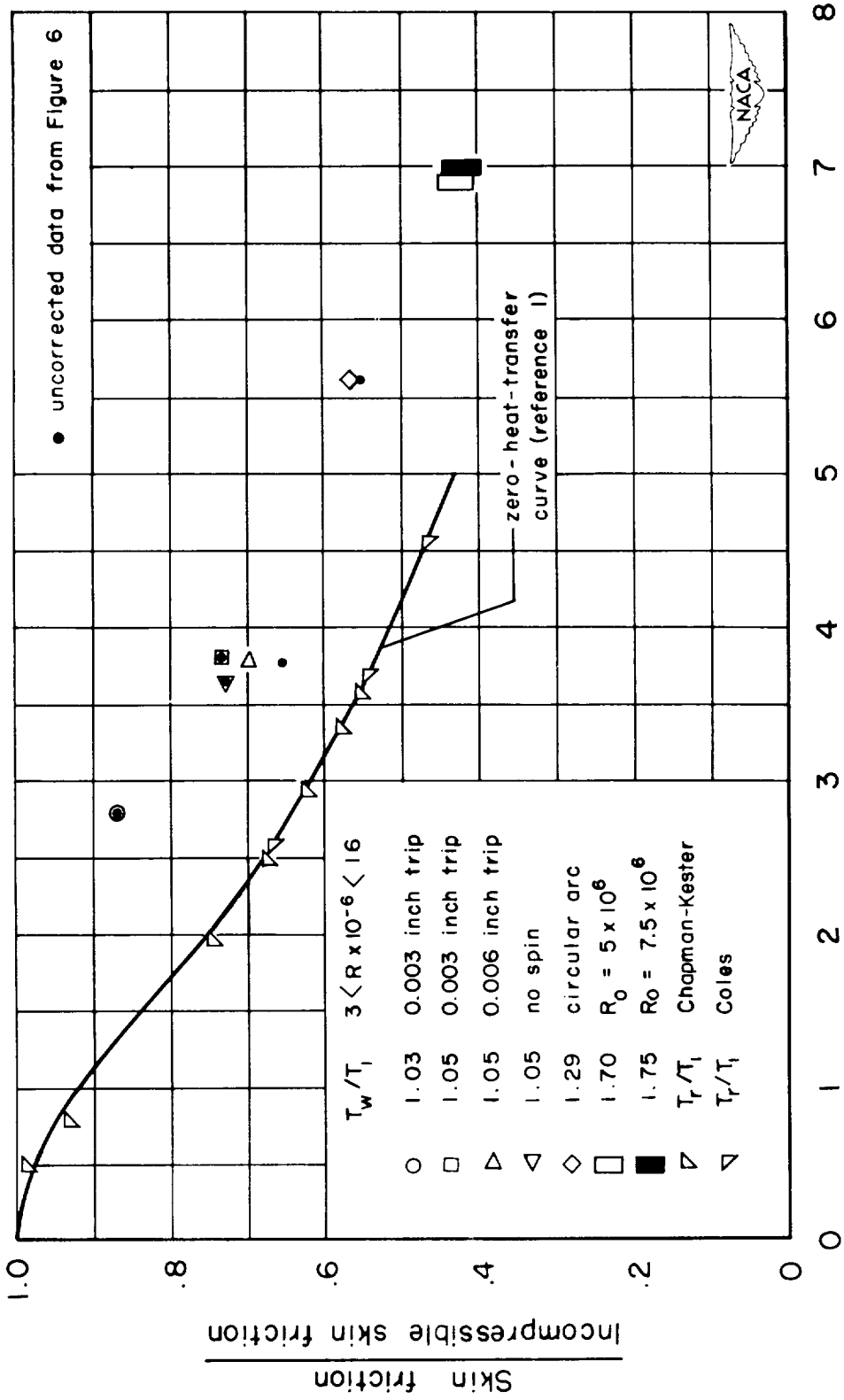

Figure 7.- Effect of Mach number on skin-friction ratio with various wall-temperature ratios, with present data corrected for boundary-layer thickening at the trip.

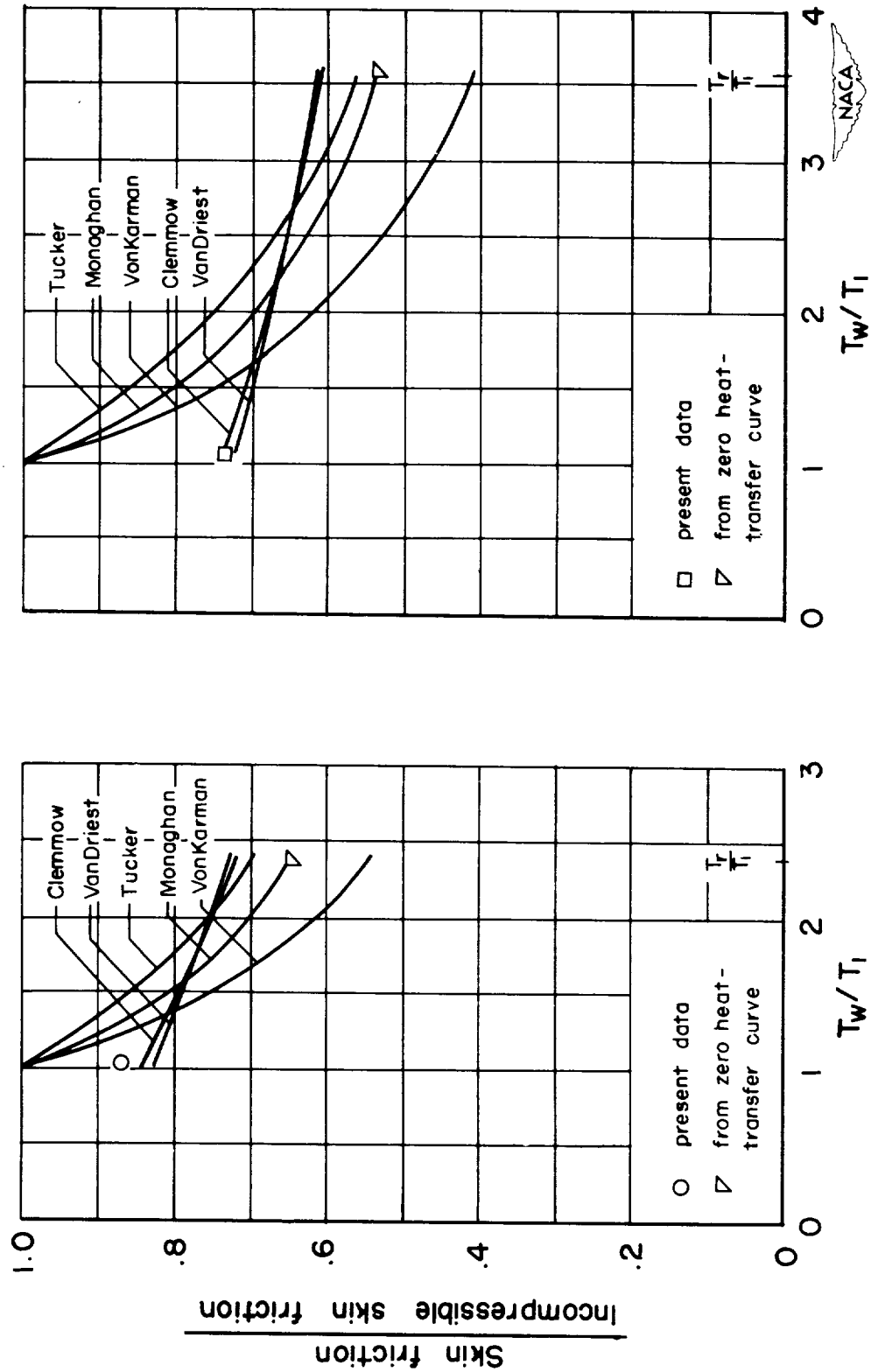

Figure 8.- Comparison of experimental and theoretical results of the effect of wall-temperature ratio on skin-friction ratio at constant Mach numbers.

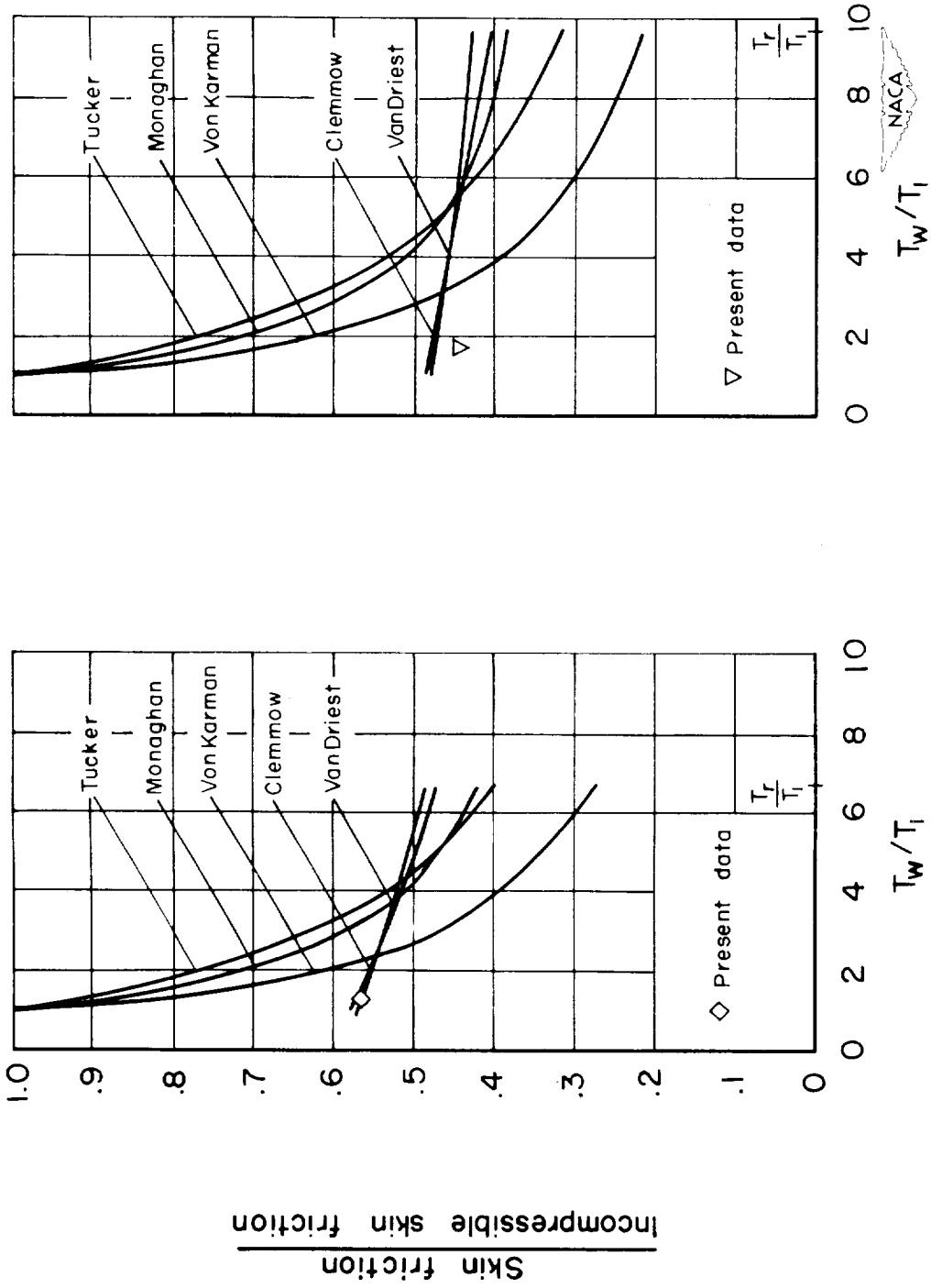

Figure 8.- Concluded.

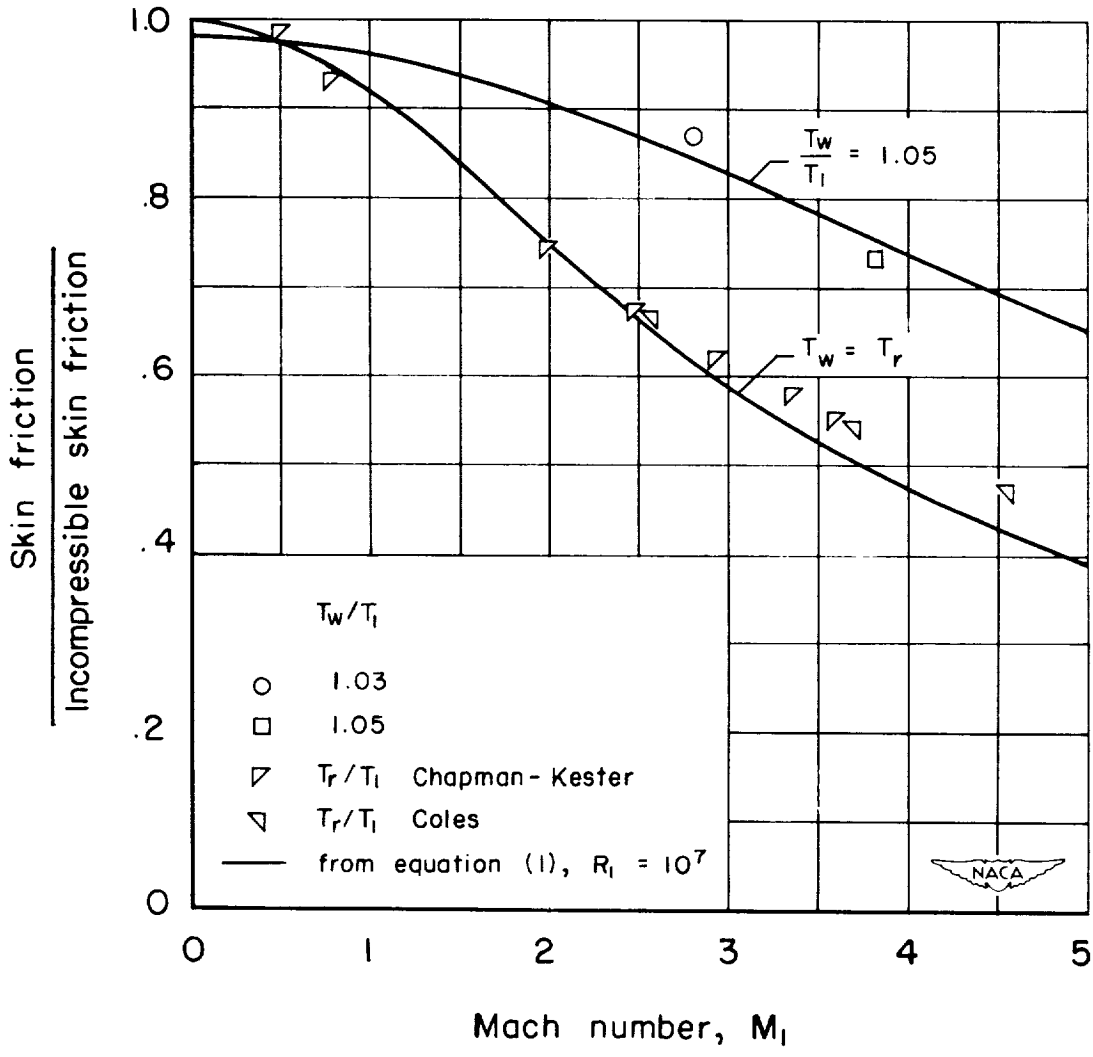

Figure 9.- Comparison of skin-fricton ratio as determined by use of equation (1) with experimental values of skin-friction ratio.

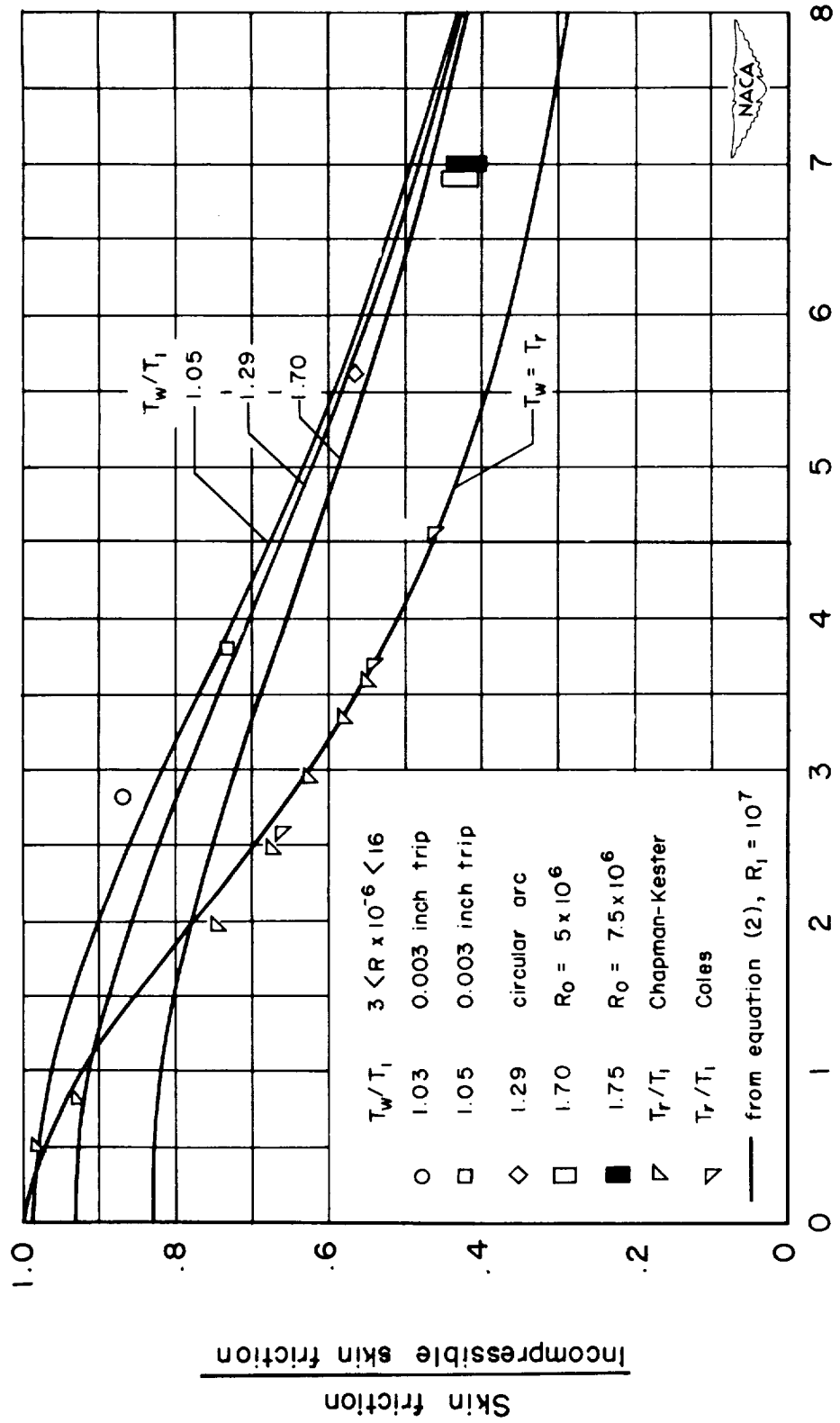

Figure 10.- Comparison of skin-friction ratio as determined by use of equation (2) with experimental values of skin-friction ratio.

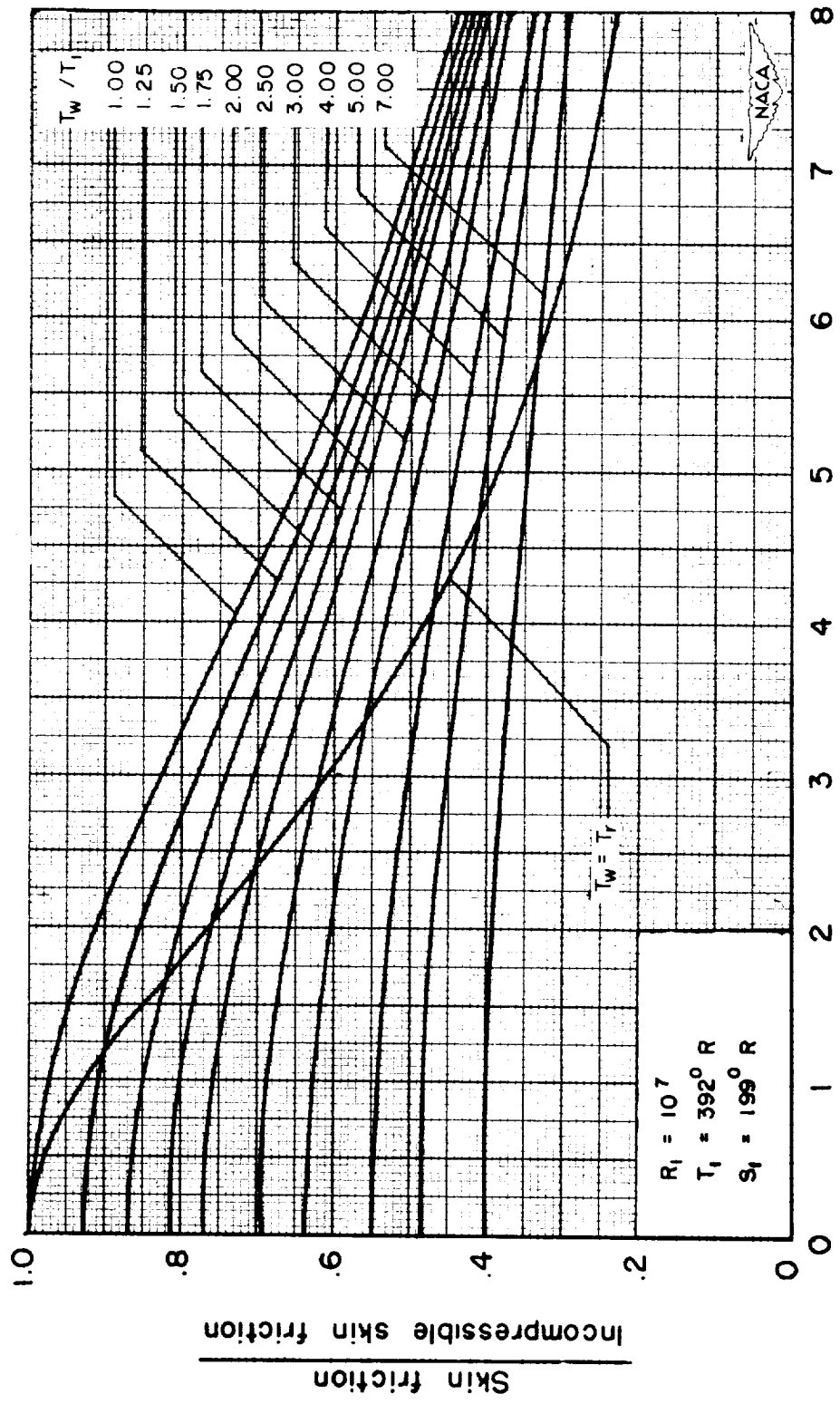

Figure 11.- Effect of Mach number on skin-friction ratio at standard isothermal altitude, as determined by use of equation (2) at constant values of wall-temperature ratio.

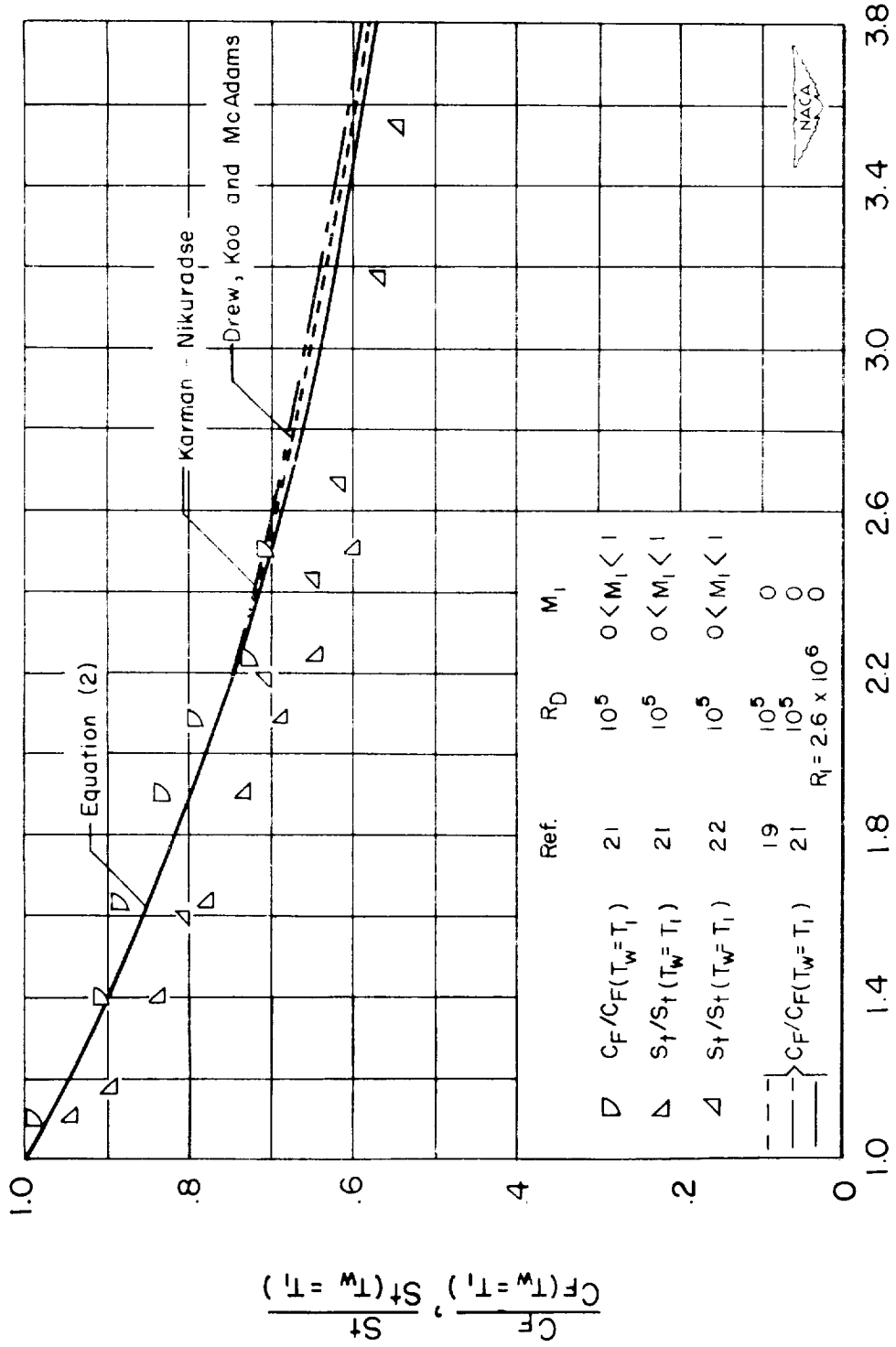

Figure 12.- Comparison of skin-friction ratio as determined by use of equation (2) with experimental and theoretical results at subsonic speeds.

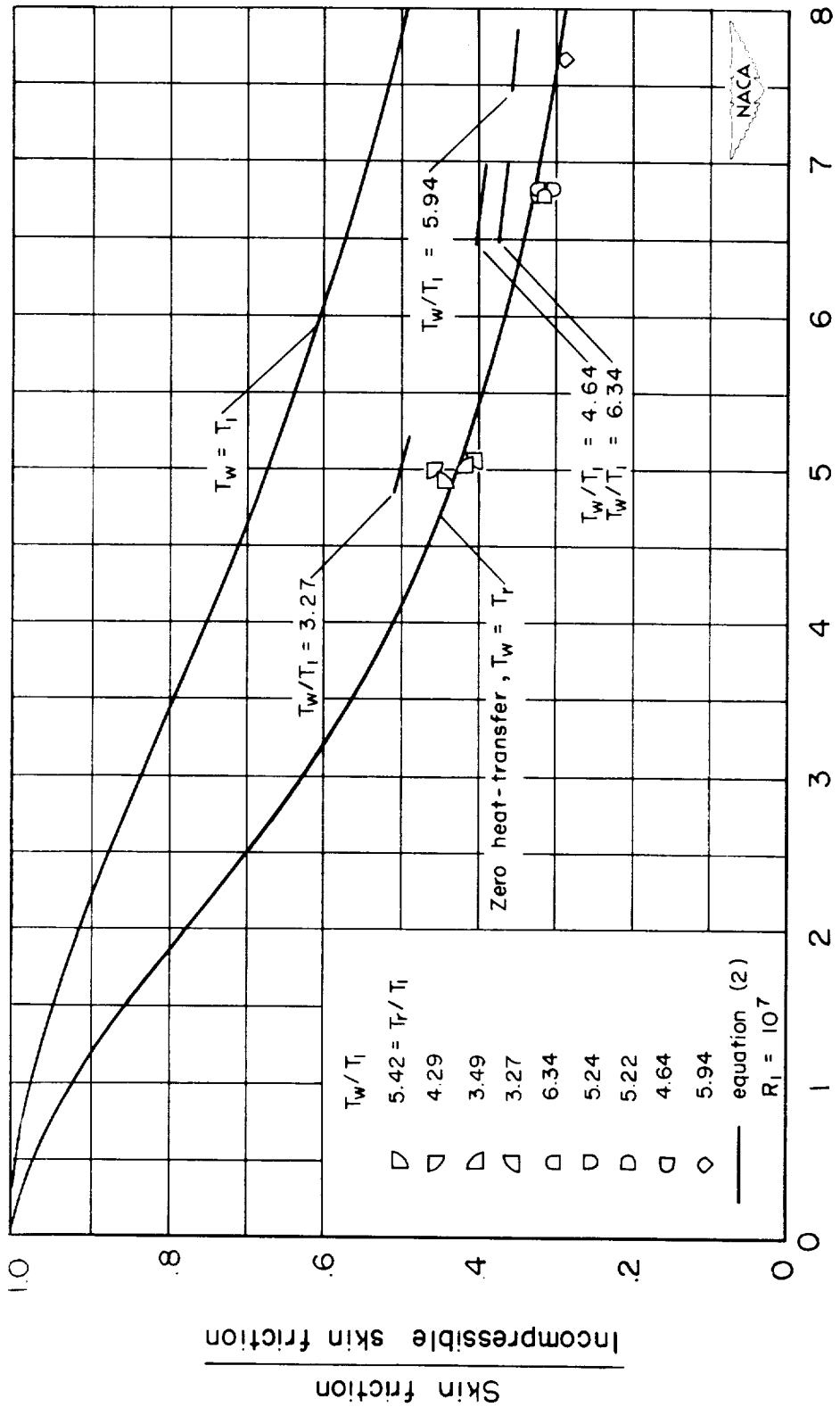

Figure 13.- Comparison of skin-friction ratio as determined by use of equation (2) with experimental results of reference 23.

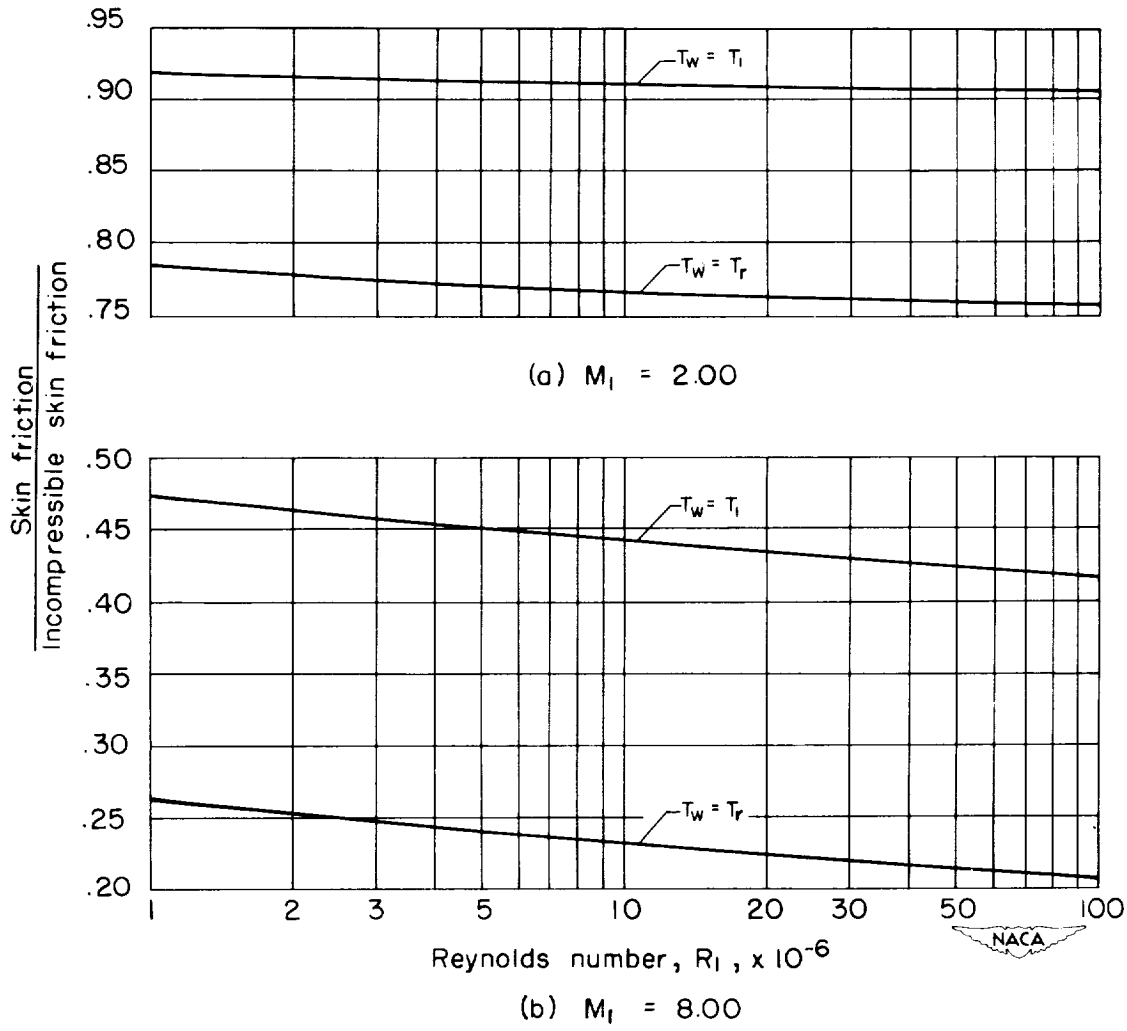

Figure 14.- Effect of Reynolds number on skin-friction ratio at standard isothermal altitude, as predicted by use of equation (2).

NACA-Langley - 3-7-55 - 1000